Summer 6-17-2011

Cyanine Dye Interactions with Quadruplex and Duplex DNA: Changes in Conformation, Stability, and Affinity

Leah E. Mickelson
Georgia State University, lmickelson1@student.gsu.edu

CYANINE DYE INTERACTIONS WITH QUADRUPLEX AND DUPLEX DNA: CHANGES IN CONFORMATION, STABILITY, AND AFFINITY

by

LEAH EVE MICKELSON

Under the Direction of Dr. W. David Wilson

ABSTRACT

There is a high demand for quadruplex-specific compounds that not only bind preferentially to quadruplex DNA over duplex DNA, but also bind to one quadruplex motif over other motifs. Quadruplex structures are recognized as common occurrences in cancer cells, and if a compound could stabilize this structure, it may serve as an effective anti-cancer treatment with minimal side effects. In this study, cyanine dyes' interactions with DNA were analyzed with fluorescence titrations, UV-Vis thermal studies, circular dichroism titrations, and surface plasmon resonance (SPR) analysis. With these techniques, binding affinity, DNA stabilization, and conformational shifts were analyzed to determine if cyanine dyes could act as quadruplex-specific binding compounds for possible cancer treatments.

INDEX WORDS: G-Quadruplex, Cyanine dyes, Thermal Melting, Circular Dichroism, Fluorescence, Surface Plasmon Resonance, Isothermal Calorimetry, Electrospray Ionization Mass Spectrometry

CYANINE DYE INTERACTIONS WITH QUADRUPLEX AND DUPLEX DNA: CHANGES IN CONFORMATION, STABILITY, AND AFFINITY

by

LEAH EVE MICKELSON

A Thesis Submitted for Partial Fulfillment of the Requirements for the Degree of

Master of Science

in the College of Arts and Sciences

Georgia State University

2011

CYANINE DYE INTERACTIONS WITH QUADRUPLEX AND DUPLEX DNA: CHANGES IN CONFORMATION, STABILITY, AND AFFINITY

by

LEAH EVE MICKELSON

Committee Chair: Dr. W. David Wilson

Committee: Dr. Kathryn Grant

Dr. Maged Henary

Electronic Version Approved:

Office of Graduate Studies

College of Arts and Sciences

Georgia State University

August 2011

DEDICATION

I would like to dedicate this work to my loving parents, who have never failed to pick me up when the skies looked gray.

Mom- You are (depending on the day) my rock and my pillow to cry into, sometimes you can be both at the same time.

Pops- I hope you know that I would never have gotten to where I am without you. Your work ethic scared me when I was younger, but as I see more and more similarities between us, it has become one more excuse for me to constantly push myself to keep working and always stay busy.

I love you both, and I promise I will make sure you get into a top-notch retirement home.

ACKNOWLEDGMENTS

I would like to acknowledge Dr. W. David Wilson who was always there to talk to about lab work, religion, and even my risk of skin cancer from too much wake boarding. I started working for Dr. Wilson during my junior year of undergraduate studies, and felt honored when he invited me to continue working with him throughout my graduate career. Thank you for your patience, guidance, and support without which I could never have gone so far.

I would also like to acknowledge Mrs. Carol Wilson. Thank you for your grammatical expertise since I missed the lessons on commas in grade school! Thank you also for always being a kind and understanding individual that always brightened a bad day.

To Rupesh Nanjuda, Nancy Kilpatrick, and Siming Wang: thank you for helping me with SPR, ITC, and MS respectively.

I would also like to thank my lab mate, Courtney Callen for always getting coffee with me so I have energy to focus in lab and for helping me remember organic chemistry substituent names. Also, thank you for being you.

Finally, I would also like to acknowledge my puppy, Gogo- she did not actively help me in any way, and in fact she was quite distracting. However, I think if she could have helped, she would have.

TABLE OF CONTENTS

LIST OF TABLES

LIST OF FIGURES

LIST OF ABBREVIATIONS

EDTA	Ethylenediaminetetraacetic acid
Tris	Tris(hydroxymethyl)aminomethane
DMSO	Dimethyl Sulfoxide
hTelo	Human telomeric DNA
c-*myc*	c-*myc* oncogene promoter
CD	Circular dichroism
MS	Mass spectrometry
ESI	Electrospray ionization
UV-Vis	Ultraviolet-visible
ΔT_m	Change in thermal melting temperature
SPR	Surface plasmon resonance
ITC	Isothermal calorimetry

Chapter 1

Introduction

The research in this thesis investigates the binding of cyanine dye derivatives with G-quadruplex DNA. It is designed to report small molecule binding affinity, mode, and specificity, as well as analyze the conformational and stability changes in quadruplex and duplex DNA.

1.1 DNA background: How and why we target it

Small molecules and proteins can be chemically tailored to bind to the minor and major grooves of DNA (see for example, Arya *et al*. work on neomycin)[1]. If strong enough interactions can be formed, it is possible to block access to the hydrogen-bonds, electrostatics, van der Waals interactions, and shape complementarity required for a particular protein to bind[2] (for example major and/or minor groove block). In some cases, we can induce topological or conformational shifts so large that the groove width or even the bending of the strand will not conform to normal cellular requirements. For this reason, DNA has been an attractive drug target: if we can stop DNA replication by targeting a unique sequence, then infectious diseases or cancer can be treated more specifically than when targeting proteins or RNA.

Current DNA targeting drugs on the market include pentamidine, berenil, and trabectadin. They can target double stranded DNA in cells by blocking in the major or minor grooves, intercalating between base pairs, and alkylating in the grooves. Many other DNA targeting drugs have been proposed, particularly in the last several years with improved instruments for DNA binding analysis. These drugs are designed to bind in the minor groove by intercalating or bis-intercalating, or interacting with the phosphate backbone[2]. Unfortunately most of these proposed

drugs have been unsuccessful due to solubility, selectivity, toxicity, transport to the nucleus or resistance problems.

1.2 The G-Quadruplex

1.2.1 Shape and corresponding sequences

Unique DNA folding motifs have been identified since Watson and Crick discovered the B-form DNA structure in 1953. Alexander Rich discovered Z-DNA in 1979, and David Davies discovered triplex DNA in 1957 and quadruplex DNA in 1962[3,4]. The G-quadruplex forms by interstrand or intrastrand guanines Hoogsteen hydrogen bonding with each other around a cation in two or more stacked guanine tetrads[5,6]. Currently, five DNA sequences are commonly investigated when considering quadruplex structures: human telomere (hTelo), c-*myc*, c-*kit*, bcl2, kras, etc[6]. Quadruplex structures form readily in G-rich single stranded DNA sequences when cations such as K^+ and Na^+ are available, so the high salt environment in the nucleus enables guanine-rich sequences to form the quadruplex structure[6]. Each of these sequences may form specific structures dependent on the direction of the phosphate backbone: parallel, antiparallel, or hybrid structures of parallel and antiparallel[7,8,9,10]. Some of these motifs are shown in Figure 1.1, but all are polymorphic and can resituate to form the most stable structure. The guanines are oriented in only anti conformation in the parallel motif, and a combination of syn and anti conformations in hybrid and antiparallel motifs[11,12,13]. Each of the structures has loops with varying numbers of base pairs and relative position along the tetrads.

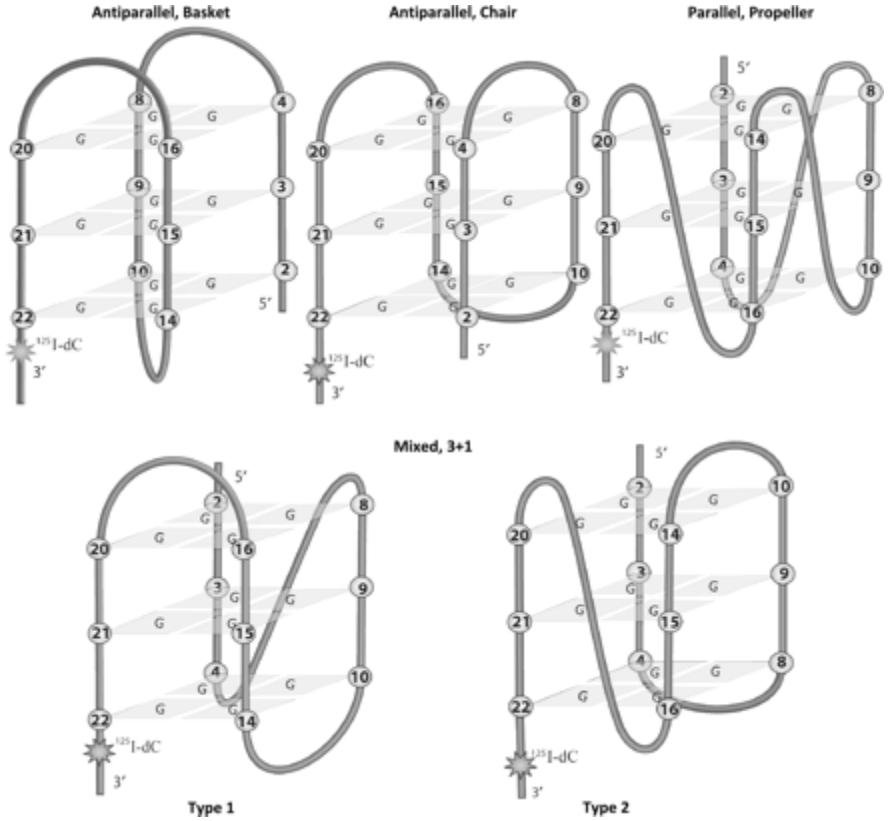

Figure 1.1 Examples of quadruplex folding motifs. Top (left to right): antiparallel basket, antiparallel chair, parallel with propeller loop. Bottom: two types of hybrid structures. All structures are polymorphic, but these appear to be the most common folding motifs[14].

1.2.2 Proposed binding modes

Using the differences between each quadruplex structure as well as the unique available interactions that separate quadruplex DNA from double stranded DNA, compounds can target the quadruplex by loop binding, end stacking, groove binding, and possibly intercalating[15,16,17]. Shown in Figure 1.2, loop binding involves indirect associations both polar and nonpolar. This typically involves stabilizing the loops, but with no real effect on the overall DNA conformation: it is typically a weak interaction and is only observed as a secondary binding mode at high concentration of ligand. End stacking utilizes primarily non-polar π-π stacking on the top or bottom tetrad; it may shift the conformation, but not significantly[18]. Groove binding occurs

when the compounds slide between the phosphate backbone, and can significantly alter the conformation by pushing the Hoogsteen bonds out of place. Finally, a compound may intercalate a quadruplex if it slides between the tetrads, greatly altering the structure and forming π-π interactions with the guanines. This is most likely too energetically expensive to occur, as the core cation must be displaced and the strands and loops get in the way in many quadruplex motifs.

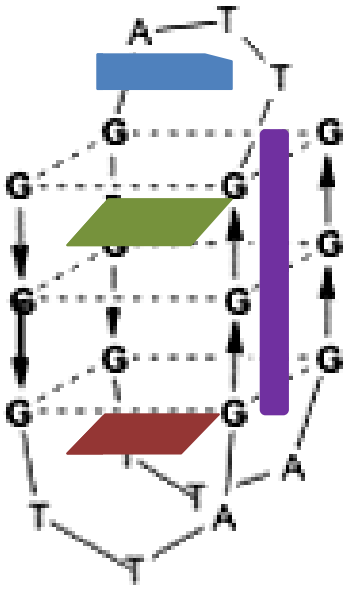

Figure 1.2 Binding modes to G-quadruplex. Blue: loop binding. Red: end stacking. Purple: groove binding. Green: intercalating.

Figure 1.2 shows an example of an antiparallel quadruplex structure with all theorized binding modes drawn in. The number of guanine tetrads and orientation of the loops will vary between quadruplex motifs, but the relative location of binding will remain consistent. That is, a loop binding compound will interact primarily with a loop, an end stacker will sit on one of the terminal tetrads, a groove binder will interact with guanines of two or more tetrads, and an intercalator will displace a cation to interact with two tetrads.

Most compounds that bind to quadruplex DNA, such as TmPyP4, RHPS4, and Braco19[18,19], have been shown to end stack. They primarily contain conjugated ring systems intended to π-π stack with the tetrads, as seen in Figure 1.3.

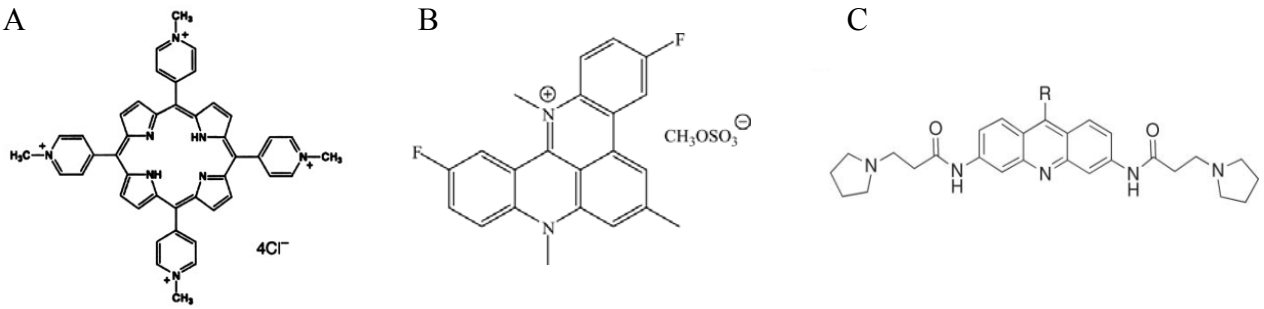

Figure 1.3 Structures of quadruplex-binding compounds. A) TmPyP4 B) RHPS4 C) Braco19

Although most quadruplex binding compounds whose binding method has been established are believed to end stack, groove binding compounds are expected to be more specific in living cells due to greater nucleic acid recognition by hydrogen bonding. That is, π-π interactions in intercalating (such as those seen in ethidium bromide) in B-form DNA are non-specific, which is why many intercalators are toxic. End stacking is also driven by π-π interactions. B-form DNA minor groove binding compounds target specific hydrogen donors and acceptors, usually those of adenine and thymine, proposed minor groove binders, such as polyamides, attempt to increase specificity by targeting guanine[20]. On this basis, targeting the gooves of quadruplex structures is highly specific, as no other DNA motifs contain alternating Hoogsteen to Watson and Crick base pairing between guanines[21].

1.2.3 Relevance to cancer

In the early 1990's, a correlation between G-quadruplex formation and cancer cells was established[22,23]. Upon further investigation, the telomere and several oncogene promoter regions were identified as sequences that form the quadruplex motif *in-vitro*. They are currently being analyzed as forming *in-vivo*, but *in-vitro* experiments are done close enough to cellular conditions that many laboratories are investigating the development of new anticancer agents by seeking quadruplex-binding compounds[24]. Cells are defined as cancer cells when they over-transcribe their DNA, causing over-replication of those cells and certain proteins within them. Additionally, the normal apoptosis command is either blocked or cannot be followed (depending on the type of cancer). Quadruplex-binding drugs can inhibit cancer cell growth in various ways, but have proved to induce apoptosis by different cues such as starving the cells of necessary proteins specific to cancer. When a sequence cannot be transcribed, the DNA can no longer form mRNA to create proteins necessary for cell functions. Quadruplex structures occur in RNA as well and RNA quadrduplex-binding drugs can induce apoptosis by different methods, but this study focuses on targeting DNA quadruplex.

In cancer cells, the nuclear protein telomerase is overexpressed, leading to a lengthened G-rich single stranded tail to each chromosome[24,25]. Telomerase is present but inactive in normal cells[26]. Under normal conditions, the length of the telomere decreases until the cell is unable to copy the DNA anymore, and the cell dies. Due to over-activation of the protein in cancer cells, the apoptosis command never occurs because there is always a long enough telomere to copy DNA. The ends of the telomere are single stranded naturally, so it must assume a conformation that stabilizes the hydrophobic nucleic acids. In normal cells, the telomere does not need to alter its conformation, but in cancer cells the proposed conformation is the hybrid quadruplex motif

seen *in-vitro*. If the quadruplex structure can be stabilized in the telomere, then it would cost too much energy for the cell to unwind it in order to add more telomere. Thus, the cancer cells could die selectively, as normal cells' telomeres are not replicated.

C-myc and *c-kit* are oncogenes and their promoter regions contain G-rich sequences[27]. They exist in all cells, but are overexpressed in cancer cells. Normally, they are read only when necessary to produce MYC and KIT proteins respectively, or to regulate gene expression. However, in cancer cells, the Watson and Crick hydrogen bonds of these sequences are broken more often to be transcribed frequently as single stranded DNA. Though these regions are double stranded, they have been found to form quadruplex structures in order to control the transcription and replication[28,29]. If the separate strands can be stabilized in the quadruplex structure, they cannot be read by transcription proteins. Then not only the overexpression would halt, but expression would entirely cease, starving the cells of MYC and KIT proteins. The cancer cells selectively die as normal c-*myc* and c-*kit* do not readily form quadruplex structures.

1.3 Cyanine dyes

Cyanine dyes are commonly used as fluorophores to monitor binding in the duplex minor groove[30,31]. The general structure involves two nitrogen-containing ring systems connected with a conjugated alkyl linker of varying odd numbers of carbons, shown in Figure 1.4.

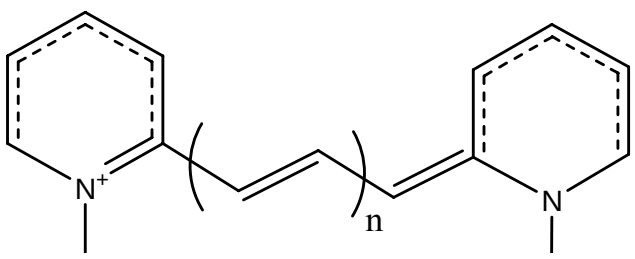

Figure 1.4 General structure of cyanine dyes

One of the ring nitrogens is positive, which helps in DNA binding. Cyanine dyes generally fluoresce above 600 nm, and are commonly used as probes to monitor DNA activity *in-vivo*[31]. Imaging of near-infrared fluorescing cyanine dyes are used in clinical studies for cancer and tumor detection[32,33,34]. Near-infrared wavelengths are less harmful to living cells: they can penetrate cell walls and be detected without residual fluorescence coming from the cell. Some of the commercially available cyanine dyes have been succesfully retained in tumor cells for weeks, but are readily excreted from normal cells[35]. Although entry into cells has been problematic for some dyes, cyanines are small and thus promising agents to detect[36] and perhaps inhibit growth of cancer cells.

The compounds under investigation are derivatives of cyanine dye structures. They have either three, five, or seven carbon linkers, and the ring systems, in this case, are primarily indolenes and benzothiozoles. Ring nitrogens have been substituted with varied functional groups in an attempt to prevent duplex binding. Quadruplex-specific binding compounds have been the focus of many studies, and have had some success in treating cancer[37,38,39]. Thus far, drugs that reached clinical studies that were developed to target G-quadruplex DNA in cancer cells have been determined to bind with proteins as well as DNA. Many have been effective against cancer, such as CX3543, but appropriate dosage cannot be determined due to excess nonspecific binding[40]. Cyanine dyes are of particular interest due to high fluorescence intensity; they can be directly monitored for binding with DNA, proteins, and entire cells. These compounds could help enrich the biological understanding of G-quadruplexes, and perhaps lead to highly specific anti-cancer agents or cancer-detecting dyes.

1.4 General methods

1.4.1 Thermal melting UV-Vis absorbance analysis

DNA folding (annealing) and unfolding (melting) can be measured using absorbance at a constant wavelength of 260 nm for duplex DNA and 295 nm for quadruplex DNA while temperature is increased. At these wavelengths, the DNAs show the greatest absorbance change and the resulting curves decrease in absorbance for quadruplex and increase for duplex DNA. Buffer composition and presence of DNA-binding compounds alter the T_m melting temperature, or midpoint between fully folded and unfolded. An increase in melting temperature in the presence of DNA-binding compounds indicates a stabilizing effect of the compound on the DNA structure. Though a large increase in T_m does not necessarily imply strong binding affinity, assessing ΔT_m (change in melting temperature) values can be used as a screening tool. Examples of melting curves for A-150 (structure shown in results section) with both quadruplex and duplex DNA are shown in Figure 1.5.

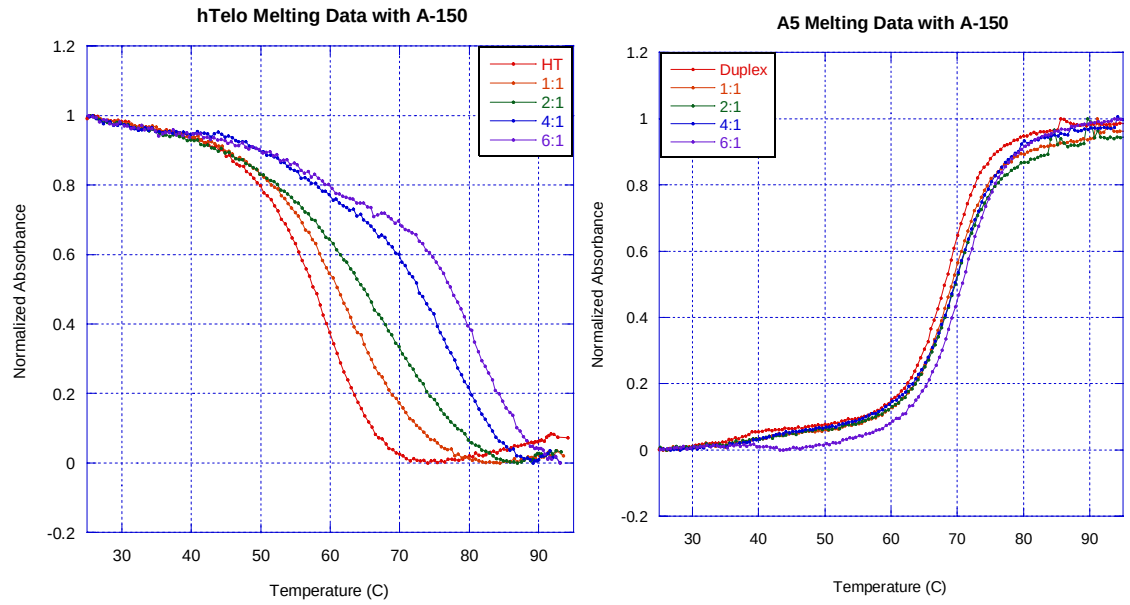

Figure 1.5 Example of quadruplex (left) and duplex (right) UV-Vis melting curves. Experiments done with 3 to 18 µM A-150 (1:1 to 6:1 ratios of compound:DNA) in Tris/K^+ buffer on a Varian Cary 300 Bio Spectrophotometer (Walnut Creek, CA) with temperature varied from 25 to 95 ˚C with 1 nm slit width. Left: 3 µM hTelo, absorbance taken at 295 nm. Right: 3 µM A_5 hairpin DNA, absorbance taken at 260 nm.

1.4.2 Fluorescence analysis

Atoms absorb energy and can emit it as heat (vibrational relaxation), fast light emission (fluorescence), or slow light emission (phosphorescence). Most compounds in this study fluoresce in response to absorption of near-infrared wavelengths of light. As compounds bind to DNA and bonds are altered, quenching or enhancement occurs, leading to a change in fluorescence emission. This change can be measured in direct correlation to DNA binding. In some cases an approximate binding constant can be determined from measuring fluorescence enhancement as DNA is titrated into a solution of fluorescent compound. Fluorescent enhancement, or the maximum emission divided by the minimum emission of the titration (compound saturated with DNA divided by free compound) at a fixed wavelength, is useful to compare DNA interactions among a family of compounds.

1.4.3 Circular dichroism analysis of DNA and compound regions

Chiral atoms rotate circularly polarized light in either dextrorototory or levorototory directions. DNA consists of chiral atoms in the backbone sugars, and as a result, different DNA structures can rotate light in different patterns. That is to say, A form, B form, Z form, triplex, and quadruplex DNA can be differentiated using circular dichroism (CD), and by studying spectral patterns[41]. Favorable DNA binding structures can be determined by observing conformational shifts as compound is titrated into a solution of DNA. DNA rotates light below 300 nm, but compounds can also rotate light if they are bound in a chiral conformation. These rotational shifts are observed in the compound region near its maximum absorbance wavelength.

1.4.4 Surface plasmon resonance (SPR)

An SPR chip contains DNA immobilized on a thin gold film by biotin or other linkages. A laser shines on the reverse side of the film, measuring the refractive index at a particular laser angle of only the gold film and anything attached to it[42]. That is, when a buffer solution flows over the film, the laser records a constant refractive index. When a compound or protein is flowed with this buffer, it may bind to the linked DNA causing a shift in refractive index and laser angle.

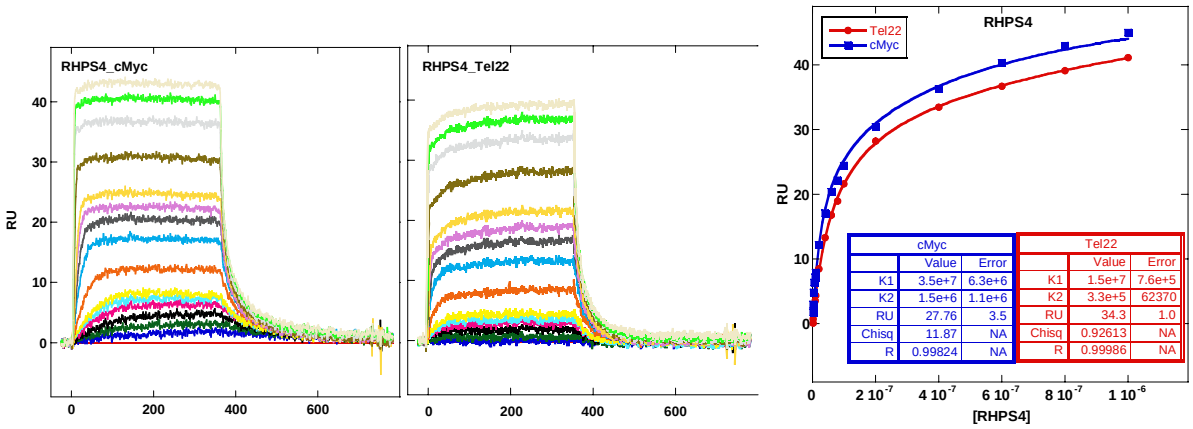

Figure 1.6 SPR sensorgrams of RU (instrument response units) vs. time and steady state response fits for RHPS4 with c-*myc* and hTelo. Biotin labeled DNAs on chip were hTelo 22, c-*myc*19, and AATT hairpin. BIAcore 2000 optical biosensor system (GE Healthcare, Sweden) was used with HEPES buffer with .01% P20. Testing was performed using regeneration buffer 10 mM glycine at pH 2.5, 200 s injection time, 400 s dissociation time, a flow rate of 25 µL/min, and a temperature of 25 ˚C. Experiment done in collaboration with Dr. Rupesh Nanjuda.

By this method, the exact binding affinity can be recorded by the SPR sensorgram by comparing the change of refractive index due to the change of contents bound to the chip. Figure 1.6 shows the SPR sensorgrams and steady state analyses of the common quadruplex-binding ligand RHPS4. The analysis shows similar binding affinities to two sequences, with slightly higher affinity to c-*myc*.

1.4.5 Binding stoichiometry analysis by mass spectrometry

Mass spectrometry is a technique in which ionized gas molecules are analyzed based on their masses and charges to attain precise molecular weights. In this project, electrospray ionization (ESI) is utilized. This method pushes a liquid solution through a tube surrounded by a current; a taylor cone is formed, ionizing, and then evaporating the liquid solution into smaller and smaller gasseous particles. The particles fly through a quadrupole and time-of-flight sorter

so that the detector will retrieve the particles at different times based on their mass to charge ratio (m/z). ESI is a gentle technique, so it allows compounds with a high enough binding constant (usually above 10^6) to remain bound to the DNA through their flight, and the resulting spectra can be analyzed to find exact binding stoichiometries of those ligands[43,44].

1.4.6 Isothermal calorimetry (ITC)

DNA binding is dependent on enthalpy and entropy, components of the Gibbs free energy. Isothermal calorimetry measures the heat absorbed (endothermic binding) or released (exothermic binding) in binding at the μcalorie level. By examining the thermodynamics of different compounds, compounds can be analyzed to determine what factors favor quadruplex over duplex DNA binding[45]. Enthalpy and binding constants are determined from measuring the heat change when compound is injected into a DNA solution, and the equations

$$\Delta G = \Delta H - T\Delta S$$

$$\Delta G = -RT\ln K$$

are used to calculate entropy and Gibbs free energy.

1.5 Goals

The goal of this study is to determine the optimum chemical features of cyanine dyes so that they will bind selectively to quadruplex over duplex DNA. Additionally, the hope is to find dyes that will bind selectively to one quadruplex motif over another. A high level of specificity in binding could ultimately lead to a low toxicity cancer treatment or cancer detecting dye to be developed from this information. Although the existence of quadruplex DNA has been known for decades, the importance of the structure has only recently been investigated. The data

collected from the variety of experimental techniques applied in this study to analyze DNA binding will enrich the growing field of quadruplex chemistry.

Chapter 2

Experimental

2.1 Materials

Three model DNA sequences were used (Figure 2.1) human telomere (hTelo), *c-myc*, and duplex (Integrated DNA Technologies, San Diego, CA). The duplex sequence with binding site GAATTC was chosen due to the A, T- rich sequence; many duplex binding compounds prefer A, T- rich sites due to a narrowing of the minor groove. The overall sequence is also a common recognition sequence, so it is a good model to use for unwanted non-specific binding.

HTelo G4 (22 mers): 5'-AGG GTT AGG GTT AGG GTT AGG G-3'

***c-myc* (19 mers):** 5'-AGG GTG GGG AGG GTG GGG A-3'

Duplex: 5'-CGG AAT TCG CTT TTG CGA ATT CGC-3'

Figure 2.1 DNA sequences tested.

All MH-, A-, and E-initialed compounds were synthesized by Dr. Maged Henary's research group (Georgia State University, Atlanta, GA). All SP-initialed compounds were synthesized by Dr. Lucjan Strecowski's research group (Georgia State University, Atlanta, GA). Finally, all In- and Q-compounds were synthesized by Dr. Bruce Armitage's research group (Carnegie Mellon University, Pittsburgh, PA). All compound structures can be seen in the results section.

The buffer used was 10mM Tris base (Fisher Scientific, Fairlawn, NJ), 50mM potassium chloride (Fisher Scientific, Fairlawn, NJ), with the pH adjusted to 7.5 with hydrochloric acid (Fisher Scientific, Fairlawn, NJ).

2.2 Thermal melting UV-Vis analysis

Six quartz cells were prepared so that the first cell was buffer, the second cell contained 3 μM DNA, and the third through sixth cells contained constant 3 μM DNA with varying ratios of compound: 1:1, 2:1, 4:1, and 6:1 in Tris/K+ buffer. The cells were scanned on a Varian Cary 300 Bio Spectrophotometer (Walnut Creek, CA) for four temperature runs: DNA melting from 25 °C to 95 °C, down to 25 °C for comparison (annealing), back up to 95 °C for melting, then finally back down to 25 °C. The scans were set at 295 nm wavelength for quadruplex sequences and 260 nm for duplex sequences, with a slit width of 1 nm.

2.3 Fluorescence titrations

A UV-Vis absorbance scan was first conducted to acquire the excitation wavelength (λ_{max}). A 5 μM solution of compound in 1 mL of Tris/K^+ buffer was scanned from 800 nm to 200 nm at a rate of 60 nm/min with a 1 nm slit width. All DNAs were diluted in Tris/K^+ buffer. The human telomere and *c-myc* DNA were annealed into a quadruplex motif by heating at 95 ˚C in the presence of potassium ions in a hot water bath for approximately five minutes, then allowing the solution to slowly cool to room temperature. Then in a fluorescence cell, an emission scan of 1 μM of compound in 1 mL of Tris buffer was taken (Varian Cary Eclipse, Walnut Creek, CA) with appropriate parameters based on the excitation wavelength. An excitation slit width of 5 nm and an emission slit width of 5 nm (these slit widths generally result in good signal to noise ratios) were used. Then, 0.05 μM of preannealed DNA was titrated into the solution and scanned under the same conditions after each addition. The solution was titrated to saturation, at which the change in fluorescence intensity was nearly zero.

2.4 Circular dichroism (CD)

A sample of pre-annealed human telomere or *c-myc* DNA was scanned with 3 μM DNA in 1 mL of Tris buffer on a Jasco J-810 Spectropolarimeter. The solution was scanned from 700 nm to 230 nm at room temperature with a scan rate of 50 nm/min and a response time of 1 second. Appropriate volumes of compound were titrated into the solution, and scanned after each addition. The instrumental program averaged two scans for each titration, then the buffer curve was subtracted using Kaleidagraph.

2.5 Surface plasmon resonance (SPR)

Fifteen solutions of compound ranging from 1 nM to 10 μM were injected over a streptavadin-coated chip containing three immobilized biotin-labeled DNA's (hTelo, c-myc, and AATT) on a BIAcore 2000 optical biosensor system (GE Healthcare, Sweden). The solutions were made with filtered and degassed HEPES buffer (10 mM HEPES, 50 mM KCl, 3 mM EDTA, pH 7.2) with .01 v/v of P20 (surfactant). A 200 s injection time, 400 s dissociation time, flow rate of 25 μL/min, and temperature of 25 ˚C were used. The regeneration buffer used was 10 mM glycine solution (30 s injection, pH 2.5). The steady state response fits were calculated using a two site fit[42]:

$$r = (K_1C_{free} + 2K_1K_2C_{free}^2)/(1 + K_1C_{free} + K_1K_2C_{free}^2)$$

where K_1 and K_2 are equilibrium constants for two types of binding sites, $r = RU/RU_{max}$, and C_{free} is the concentration of the compound in equilibrium with the complex which is fixed by the concentration in the flow solution.

2.6 Electrospray ionization mass spectrometry

A sample of concentrated c-*myc* was desalted in 0.1 M ammonium acetate buffer (Fisher Scientific, Fair Lawn, New Jersey) pH 6.8 to prevent sodium adduct peaks. A dialysis bag was

prepared with DNA, and the solution was allowed to sit, chilled for at least seven days during which the buffer solution was changed every other day. Solutions were made with 10 μmol c-*myc* in ammonium acetate buffer with 10% methanol (Fisher Scientific, Fair Lawn, New Jersey) with varying ratios of compound to DNA: 0:1, 1:1, 2:1, 4:1, and 6:1. The solutions were tested on the Waters Micromass Q-TOF micro in negative ion mode with a capillary voltage of 2500 V.

2.7 Isothermal calorimetry

Solutions of compound (0.2 mM) were injected 30 times into solutions of DNA (0.02 mM). All solutions were degassed at 25 °C for 15 minutes. TRIS/K^+ buffer was used in the reference cell. The injections were monitored at 25 °C with a reference power of 1 μcal/s, an initial delay of 300 s, and a stirring speed of 290 (VPC-ITC). The first injection was 2 μL for 4 sec, with a spacing of 300 s, and a filter period of 1 s. The remaining 29 injections were 10 μL volume for a duration of 20 s, with a spacing of 300 s, and a filter period of 1 s. The data was analyzed by VPViewer 2000 software.

Chapter 3

Results on Families of Compounds

3.1 Benzothiozole cyanine dyes

Benzothiozole cyanine dyes are known to bind to duplex DNA, forming hydrogen bonds in the minor grooves: sulfurs with the bases and nitrogens with the backbone. This study includes some benzothiozole dyes with varied nitrogen substituents and linker systems. The general structure of the dyes tested is shown in Figure 3.1. In general, these compounds prove to bind weakly with minimal selectivity to quadruplex sequences. However, several binding trends are identified. The structures and thermal melting data are shown in Table 3.1.

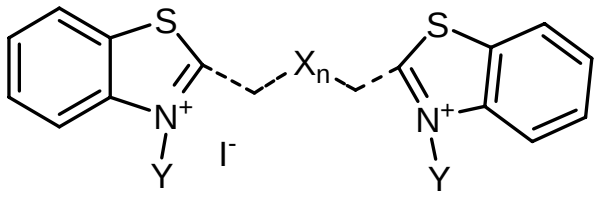

Figure 3.1 General structure of benzothiozole cyanine dyes synthesized by Dr. Strekowski *et al* (Georgia State University, Atlanta, GA).

Table 3.1 Benzothiozole dyes thermal melting data (ΔT_m) with hTelo (°C)

	hTelo				Duplex			
	1:1	**2:1**	**4:1**	**6:1**	**1:1**	**2:1**	**4:1**	**6:1**
SP-1-2 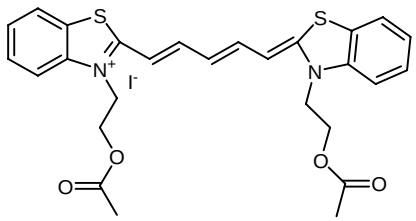	0.6	1.3	2.7	3.7				
SP-1-25 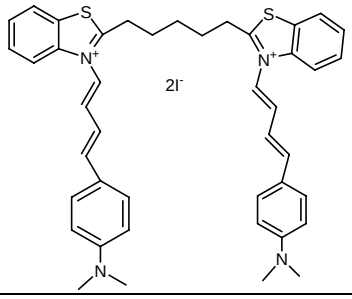	0.6	0.6	1.1	*				
SP-1-26 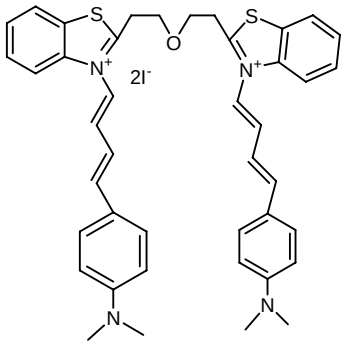	0.4	3.1	5.6	6.6				
SP-1-27 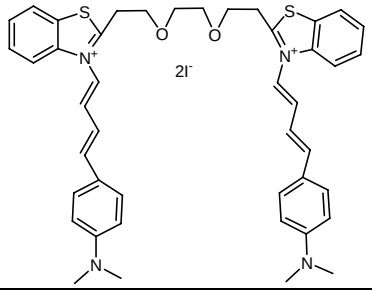	0.0	2.1	5.7	4.7				
SP-1-28 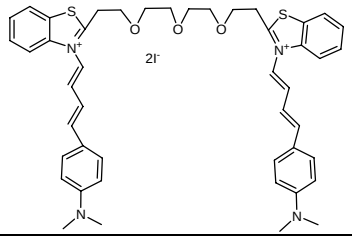	0.0	0.6	0.6	1.6				

SP-1-79 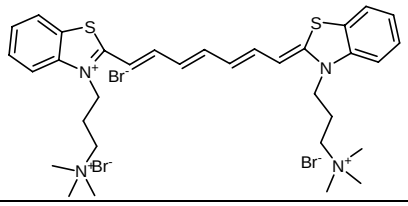	2.6	5.6	13.1	17.8	0.4	3.4	8.5	12.5
SP-1-80 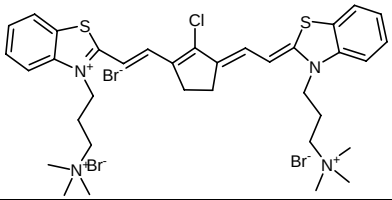	0.6	0.2	0.7	0.2	0	2	1.2	0.2
SP-1-93 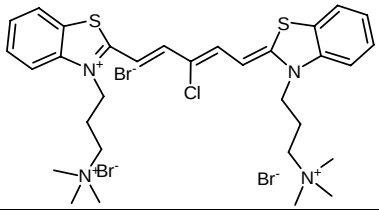	0.6	4.2	17.6	22.7	9.0	12.0	12.1	13.1
SP-1-98 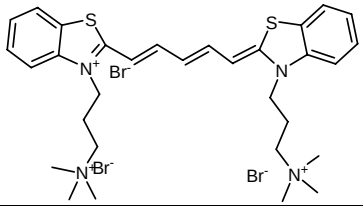	4.5	10.0	15.1	19.1	5.6	6.1	11.0	12.0
SP-1-99 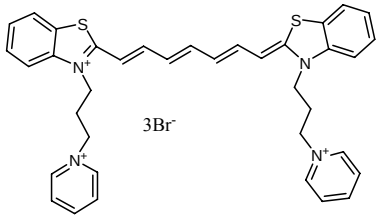	0.9	0.9	2.4	4.0	3.0	9.2	9.2	10.5
SP-1-116 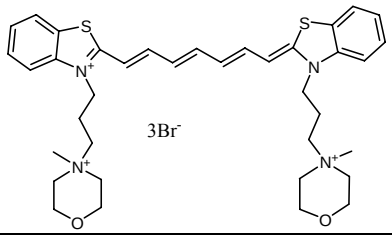	0.0	0.7	0.8	1.8	1.9	2.8	8.6	9.8

SP-1-117 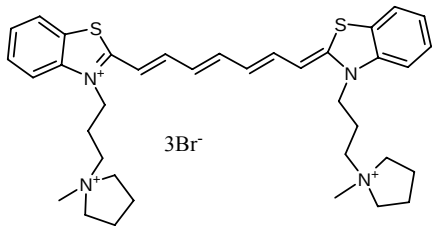	-0.8	-0.3	0.2	1.4	0.0	0.1	-0.9	0.2
SP-1-149 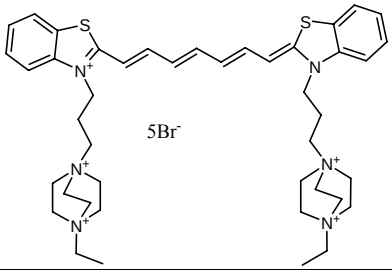	0.4	0.6	16.9	>30	0.0	12.0	14.1	12.2
(Error is ± 1 ˚C) Note: Some compounds were not tested with duplex due to poor stabilization of quadruplex.								

Thermal melting shows that stabilization of the quadruplex is dependent on both the linker as well as the substituents. That is, when comparing SP-1-79 (heptamethine linker) to SP-1-98 (pentamethine linker), it appears that the shorter linker length fits the shape of the quadruplex to induce a better stabilization. This is supported by the thermal melting results of SP-1-80, which is far more rigid with the linker ring so the compound cannot bend to fit the DNA shape; the binding drops to nearly zero. When chlorine is attached on the pentamethine linker, as in SP-1-93, the stabilization increases even further. Finally, looking at SP-1-79 compared to ring substituent alterations SP-1-99, SP-1-116, and SP-1-117, the cationic substituent appears to stabilize best when it has the small trimethyl amine substituent. No error is shown for thermal melting data because it is used as a screening tool; the error is approximately ± 1 °C, but enough solutions are tested for each compound that an approximate stabilization is determined.

Dyes with longer linker lengths tend to be sensitive to heat and light: SPR was attempted on many of these compounds, but they bind too poorly to obtain accurate fits. Fluorescence titrations confirm binding; the titration of hTelo into a solution of SP-1-93 is shown as an example in Figure 3.2. A slight red shift and a fluorescence enhancement of 2.3 are observed.

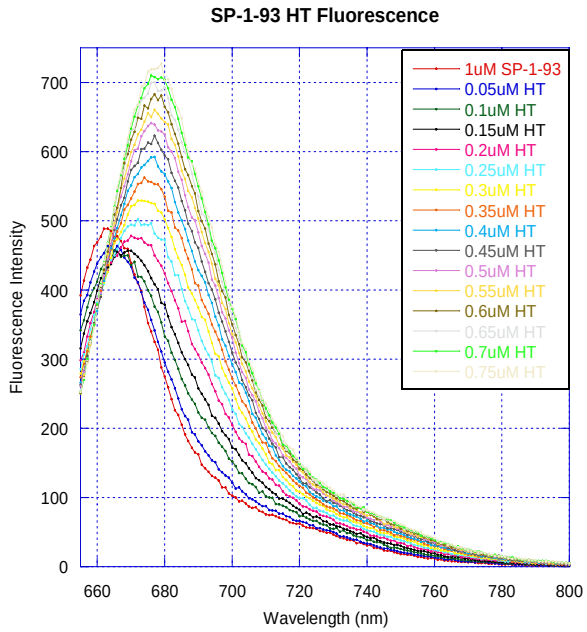

Figure 3.2 Results of fluorescent titration on Varian Cary Eclipse (Walnut Creek, CA) in TRIS/K^+ buffer. Slit widths were 5 nm (ex) and 5 nm (em). λ_{ex} was 630.0 nm and λ_{em} was taken from 650 nm to 800 nm. 1µM SP-1-93 was titrated with 0.05µM increments of hTelo. Fluorescence enhancement was 2.3.

3.2 Asymmetric Cyanine Dyes

Asymmetric cyanine dyes tested in this study include an indolene linked to an isoquinoline by a trimethine linker. The nitrogen substituents are varied with sulfonate, carboxyl, and trimethyl amine groups. The general structure is shown in Figure 3.3. At the experimental pH, the sulfonate and carboxyl substituents are negative in solution, lessening the overall charge, and based on the thermal melting data shown in Table 3.2, weakening the stabilization of quadruplex DNA.

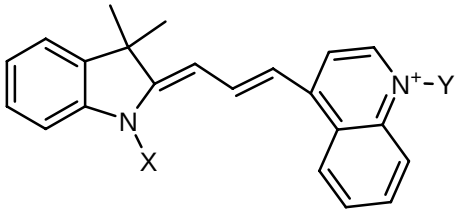

Figure 3.3 General structure of asymmetric cyanine dyes. Synthesized by Dr. Bruce Armitage *et al.* (Carnegie Mellon University, Pittsburgh, Pennsylvania).

Table 3.2 Asymmetric dyes thermal melting data (ΔT_m) with hTelo (°C)

	1:1	2:1	4:1	6:1
InQ(3)PRO 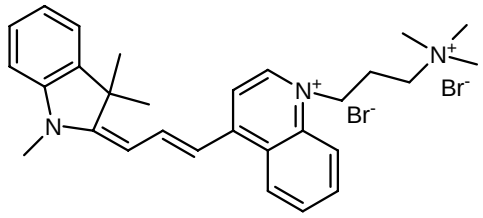	4.9	4.8	11.5	15.5
InQ(3)PROSO$_3^-$ 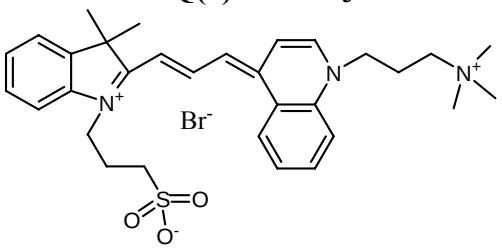	0.6	1.6	2.2	5.2
InQ(3)PROCOO$^-$ 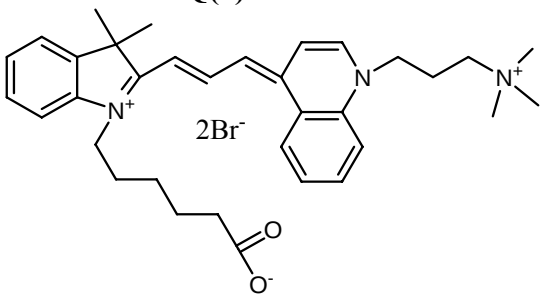	0.6	0.6	2.5	2.7
InQ(3)SO$_3^-$ 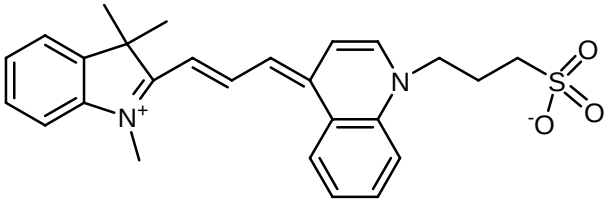	0.6	2.1	0.6	1.2
(Error is ± 1 ˚C)				

Fluorescence titrations support the melting stabilization for InQ(3)PRO, InQ(3)PROSO$_3^-$, and InQ(3)PROCOO$^-$, but differed with InQ(3)SO$_3^-$ as shown in Table 3.3. While InQ(3)PRO and even InQ(3)PROSO$_3^-$ show some DNA conformational shift (Figure 3.4), the CD titration of InQ(3)SO$_3^-$ shows no DNA change. Therefore, the fluorescence change is most likely due to stacking of compound on the DNA[46]. All of these dyes show nearly no fluorescence when free in solution, so the large enhancement is due to a small initial fluorescence intensity.

Table 3.3 Asymmetric dyes fluorescence enhancement ($F_{saturated}/F_{compound}$) with hTelo

InQ(3)PRO	52.8
InQ(3)PROSO$_3^-$	3.5
InQ(3)PROCOO$^-$	6.2
InQ(3)SO$_3^-$	15.8

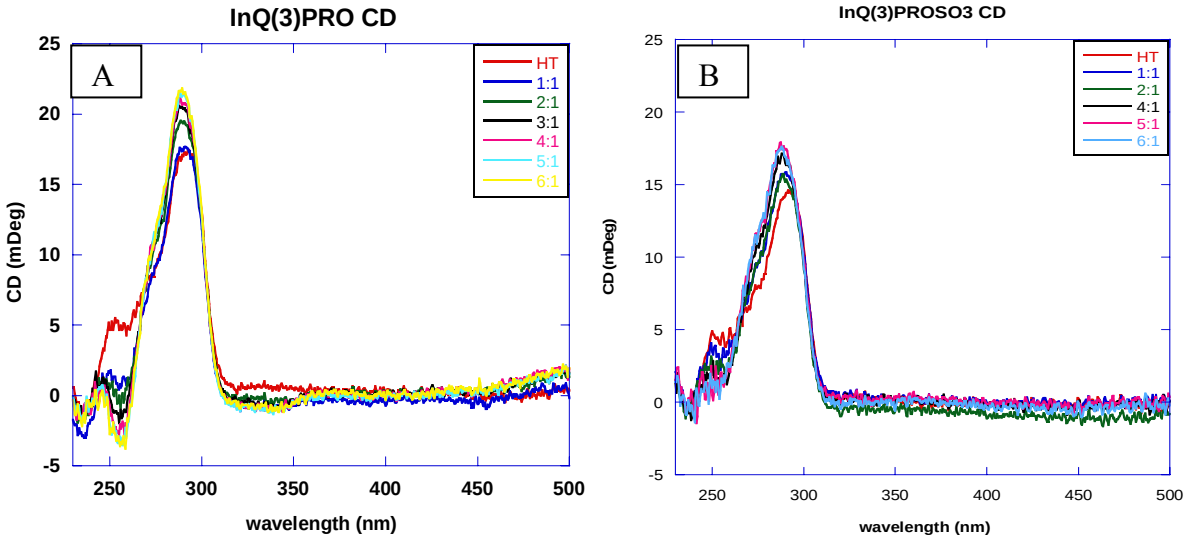

Figure 3.4 CD titrations done with 3µM DNA on the Jasco J-810 Spectropolarimeter in Tris/K+ buffer. The solution is scanned from 230 nm to 700 nm at 25 ˚C with a scan rate of 50 nm/min, slit width of 1 nm, and a response time of 1 second. 3µM of MH-5 was titrated for each scan. A) Titration of InQ(3)PRO into hTelo. B) Titration of InQ(3)PROSO$_3^-$ into hTelo.

Shown in Figure 3.5, the SPR steady state response fit confirms some binding to both quadruplex structures, but proves to be extremely weak and difficult to fit to a specific model. Although the two methyl groups on the indolene group seem to block duplex binding (based on thermal melting and SPR studies), the quadruplex binding with these compounds is clearly weak (less than 10^6 M^{-1}).

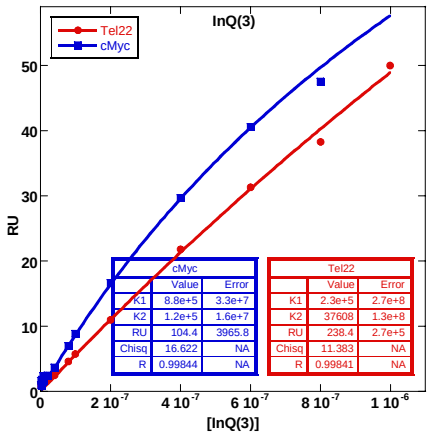

Figure 3.5 SPR steady state response fits for InQ(3)PRO with c-*myc* and hTelo. Biotin labeled DNAs on chip were hTelo 22, c-*myc*19, and AATT hairpin. BIAcore 2000 optical biosensor system (GE Healthcare, Sweden) was used with HEPES buffer with .01% P20. Testing was performed using regeneration buffer 10 mM glycine at pH 2.5, 200 s injection time, 400 s dissociation time, a flow rate of 25 µL/min, and a temperature of 25 ˚C. Experiment done in collaboration with Dr. Rupesh Nanjuda.

3.3 Indolene cyanine dyes

A number of symmetric indolene cyanine dyes were tested, and they expanded on results from the benzothiozole and asymmetric cyanine dyes. The two methyl groups on the indolene ring systems prove to essentially eliminate duplex binding (of the sequences tested), and any negatively charged groups prove to consistently limit binding to both quadruplex and duplex.

3.3.1 Trimethine cyanine dyes

The general structure of the trimethine dyes used in this study is shown in Figure 3.6.

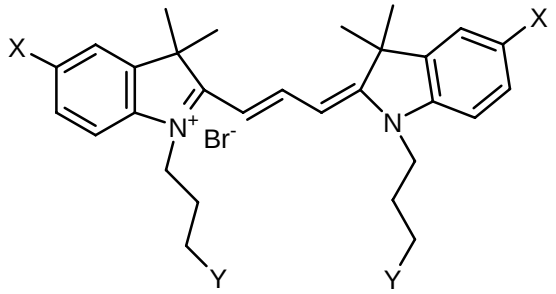

Figure 3.6 General structure of trimethine dyes synthesized by Dr. Henary *et al* (Georgia State University, Atlanta, GA).

Although there are many successful compounds in this study, binding progress required narrowing down substituents that eliminate quadruplex binding, duplex binding, or both. Thermal melting data shown in Table 3.4 clearly demonstrates sulfonate and carboxyl groups on any part (ring systems, linker, or, sidechains) of the cyanine dye structure eliminate binding to both types of DNA. DNA is a highly negative structure, and quadruplex is tightly packed with negative charges. Sulfonate and carboxyl groups are negatively charged at the buffer pH, and repel the compound from its target sequence. The thermal melting data also demonstrates slightly negative ΔT_m values (a minor destabilization of the quadruplex structure) in the cases of E-4 and E-8 which both contain aromatic sidechains: large ring nitrogen substituents also showed poor binding for benzothiozole compounds. This destabilization is most likely due to both the lessened overall charge as well as the hydrophobic substituents.

Table 3.4 Trimethine dye thermal melting (ΔT_m) data (°C)

	Human Telomere				Duplex			
	1:1	**2:1**	**4:1**	**6:1**	**1:1**	**2:1**	**4:1**	**6:1**
MH2 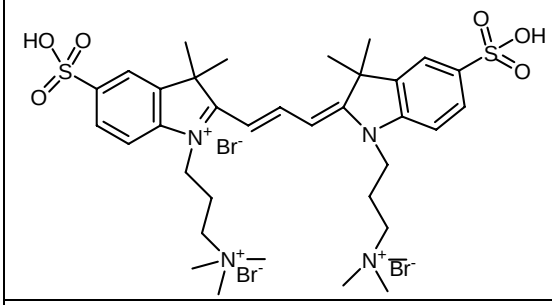	1.5	1.1	0.6	1.2				
A-80 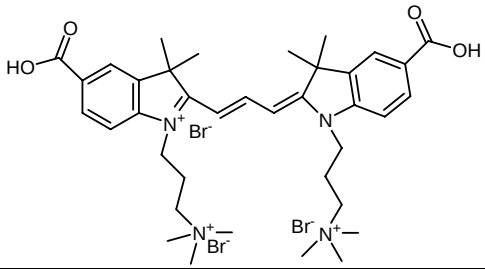	0.6	1.1	2.6	7.2				
E-4 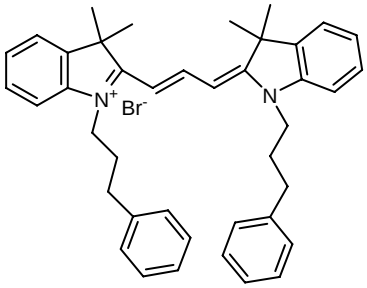	1.0	1.6	-3.9	*				
E-6 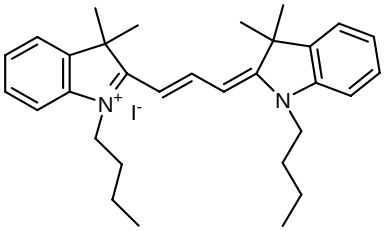	0.6	0.1	0.2	*				

E-8 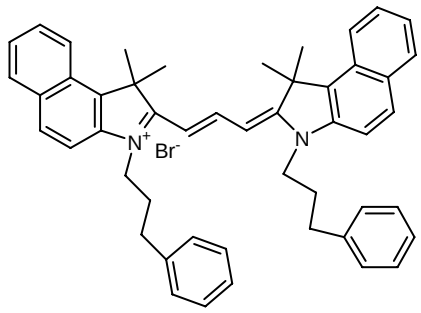	0.0	-0.4	-1.4	-4.3				
MH-4 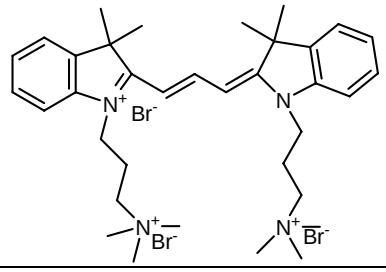	1.6	4.1	8.7	13.7	0	0.9	-0.2	1.8
MH-5 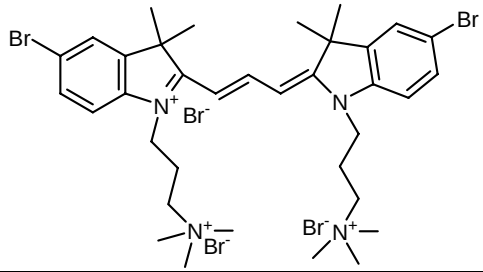	1.0	5.2	14.2	23.7	-0.1	-1.0	-1.0	-0.1
A-138 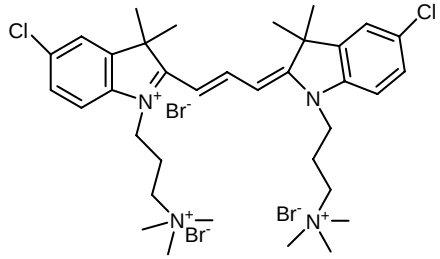	3.0	7.0	14.6	*	0.0	0.0	-1.0	*
A-134 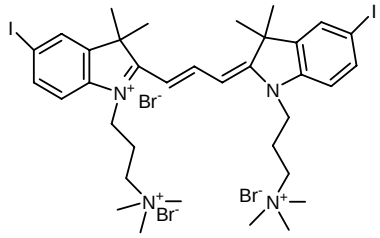	2.6	6.6	17.2	20.8	1.0	1.1	1.1	*

* Experiment showed too much noise to accurately calculate T_m
(Error is ± 1 ˚C)
Note: Some compounds were not tested with duplex due to poor stabilization of quadruplex.

Based on the melting temperature data, halogens linked onto the indolene ring systems prove to greatly increase stabilization among these compounds. Trimethine compounds increase in DNA stabilization as the attached halide increases in size. These compounds consistently bind well to quadruplex and have nearly no binding to duplex A, T-rich sequences. 4:1 ratios are considered in analyzing binding due to assumed binding site saturation based on presumed two-site binding. As thermal melting data is best analyzed as a screening tool, multiple compound to DNA ratios are tested, but the 4:1 ratio is compared to maintain consistency. In many cases, ΔT_m values continue to increase steadily until 6:1 compound to DNA ratio when interacting with hTelo. This may be indicative of compounds self stacking along the DNA. SPR confirms that despite aggregation problems, the compounds bind better to hTelo than to duplex DNA, but still with binding constants less than 10^7 M^{-1}. However, the compounds are found to bind strongly to c-*myc* as seen in SPR steady state response fits in Figure 3.7 ($K>10^6$ M^{-1}). Thermal melting data is difficult to collect accurately for c-*myc* due to its high melting temperature. Compounds often increase the melting temperature beyond measurable values with this DNA. Salt concentrations may be lowered to decrease the c-*myc* melting temperature, but cellular conditions as well as quadruplex formation require salt. Thus, lowering salt concentrations is not always a desirable comparison. Nonetheless, a strong correlation is observed between thermal melting screening data and SPR proven binding affinities to c-*myc*.

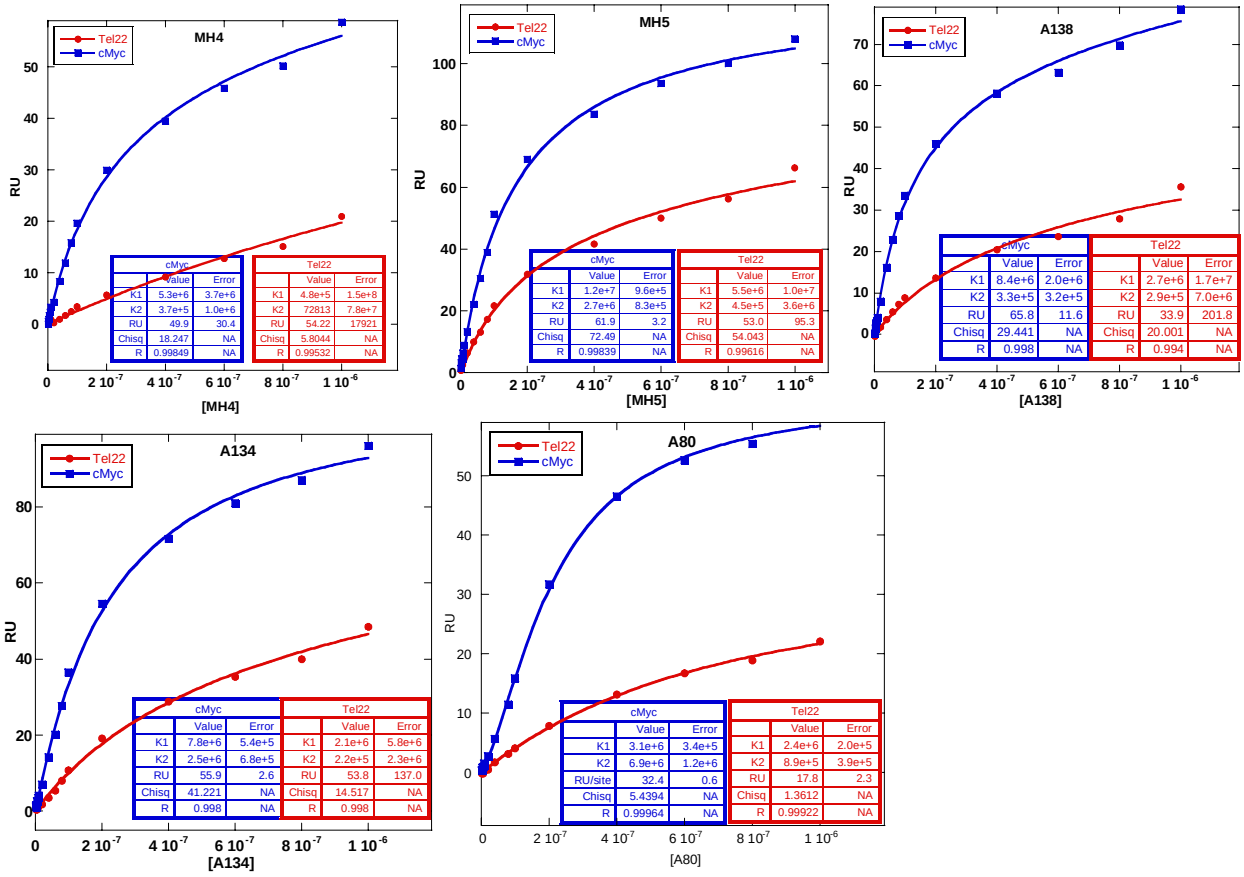

Figure 3.7 SPR steady state response fits for trimethine dyes with c-*myc* and hTelo. Biotin labeled DNAs on chip were hTelo 22, c-*myc*19, and AATT hairpin. BIAcore 2000 optical biosensor system (GE Healthcare, Sweden) was used with HEPES buffer with .01% P20. Testing was performed using regeneration buffer 10 mM glycine at pH 2.5, 200 s injection time, 400 s dissociation time, a flow rate of 25 µL/min, and a temperature of 25 ˚C. Experiment done in collaboration with Dr. Rupesh Nanjuda.

No trend in fluorescence enhancement can be distinguished, as demonstrated in Table 3.5. All dyes increase emission far more when titrated with c-*myc* than with hTelo, but exact enhancement is primarily dependent on free compound fluorescence emission (minimum fluorescence intensity). All of these dyes show very high fluorescence intensities, and increase to nearly (and sometimes over) the amount of emitted light that the fluorometer detects under the standard assay. All compounds increase fluorescence intensity when bound to DNA. MH-5 fluorescence titrations are shown in Figure 3.8.

Table 3.5 Fluorescence enhancement ($F_{saturated}/F_{compound}$) of trimethine dyes

	hTelo	c-*myc*
MH4	1.7	7.7
MH5	1.6	4.6
A-138	2.7	5.4
A-134	2.0	4.1
A-80		1.39

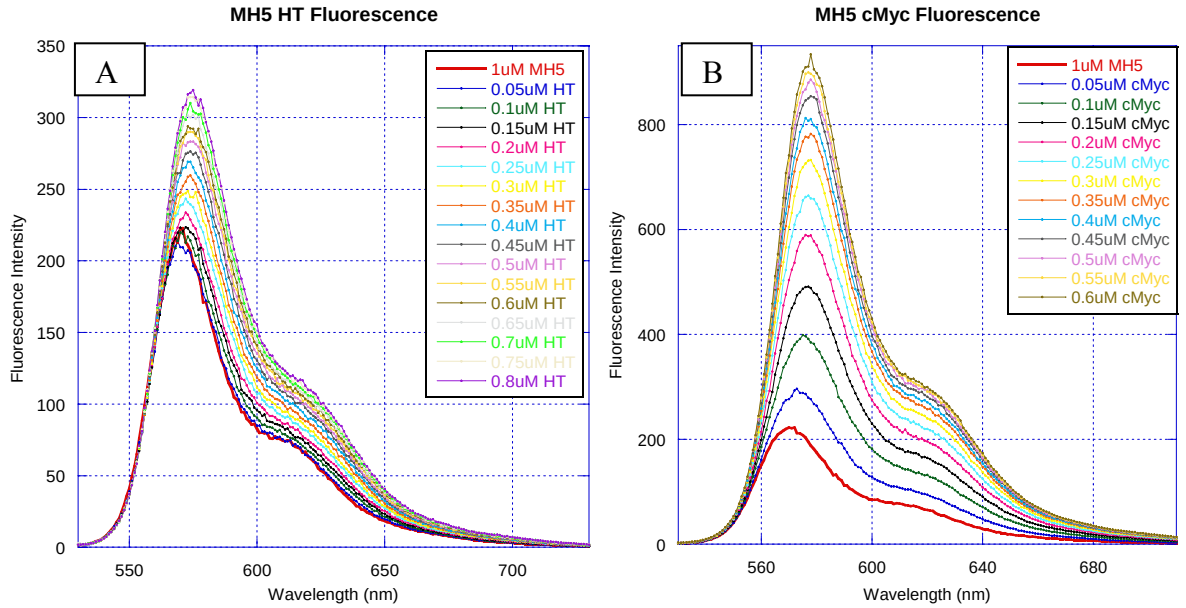

Figure 3.8 Results of fluorescent titration on Varian Cary Eclipse (Walnut Creek, CA) in TRIS/K^+ buffer. Slit widths were 5 nm (ex) and 5 nm (em). λ_{ex} was 520.5 nm and λ_{em} was taken from 530 nm to 730 nm. A) 1µM MH-5 titrated with 0.05µM increments of hTelo. B) 1µM MH-5 titrated with 0.05µM increments of *c-myc*.

Isothermal Calorimetry (ITC) experiments were performed to test the SPR and fluorescence preference in binding c-*myc* over hTelo. ITC is known to under-estimate binding constants for strong binding compounds in comparison with other techniques such as SPR, which is true for these compounds shown in Figure 3.9 with corresponding results shown in Table 3.6. These tests consistently show a single binding site, which is inconsistent with the equation that

best fits the SPR data. ITC measures heat from binding, so a second, or perhaps nonspecific binding site may show no heat change. Mass spectrometry proves this assumption to be correct. Shown in Figure 3.10, one binding site is preferred, but a second binding site can occur in high compound to DNA ratio conditions.

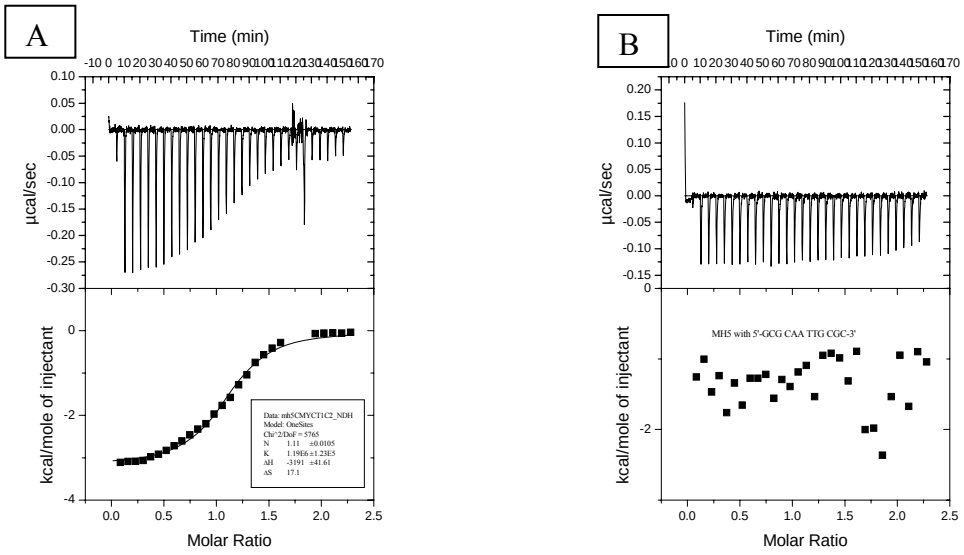

Figure 3.9 ITC Titrations of 0.2 mM MH5 into 0.02mM DNA. VPC-ITC with VPViewer 2000 software was used. Reference cell and solutions contained TRIS/K^+ buffer. 30 injections were measured at 25 ˚C with reference power of 1 µcal/sec and 300 s spacing time. A) c-*myc* B) AATT duplex. Experiment done by Nancy Kilpatrick.

Table 3.6 Thermal data for MH-5 binding

Oligomer	**Stoichiometry**	**K (M^{-1})**	**Δ H (cal/mol)**	**Δ S (cal/mol C^o)**	**Δ G (cal/mol)**
c-*myc*	1.11 ± 0.01	1.19E+06	-3190 ± 40	17.1	-8278.85
hTelo	Weak binding- unable to fit				
A_2T_2	No binding				

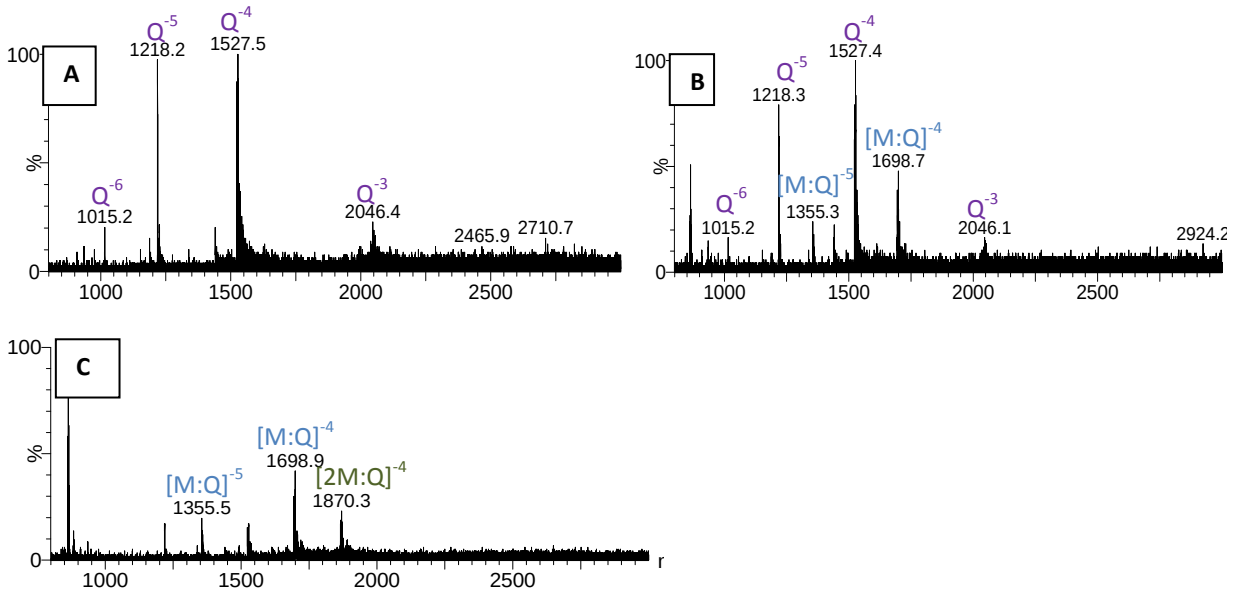

Figure 3.10 Electrospray Ionization mass spectrometry results from Waters Micromass Q-TOF micro in ammonium acetate buffer. Spectra taken in negative mode with voltage of 2500 mV. MH5 with c-*myc* mass spectra with 10% methanol. A) 10µM c-*myc* B) 2:1 ratio C) 4:1 ratio.

Circular dichroism experiments are done to determine binding mode, but, the spectra consistently show nearly no spectral changes in the DNA region. However, the dihalogenated compounds consistently show an induced CD in the dihalogenated compounds' absorbance region, shown in Figure 3.11. This is most likely due to self stacking as cyanine dyes are known to do, so the CD ratio is not the binding ratio; the compound chirality may change as the compounds stack on the quadruplex, but these are weak interactions due to the high compound to DNA ratio. When compounds are titrated into an hTelo solution, a small shift from hybrid to antiparallel structure is observed. In addition, a large induced CD is observed that saturates at an 8:1 compound to DNA ratio. Due to confirmed 2:1 binding, this can only result from compounds stacking as J- or H-aggregates. A compound-only CD titration was done to determine if the compounds are stacking in solution or with the DNA: no induced CD is observed. Therefore, the compounds must aggregate on DNA with low stability so they do not

remain stacked in the ionized gas form required of mass spectrometry. A slight positive induced CD is seen in titrations with c-*myc*, but no change is observed in the DNA region indicating that the compounds do not alter the conformation of c-*myc*, and only stabilizes the antiparallel form of hTelo. Loop binding and sometimes end stacking are recognized as binding modes that disturb structures the least, but stacking usually occurs along grooves.

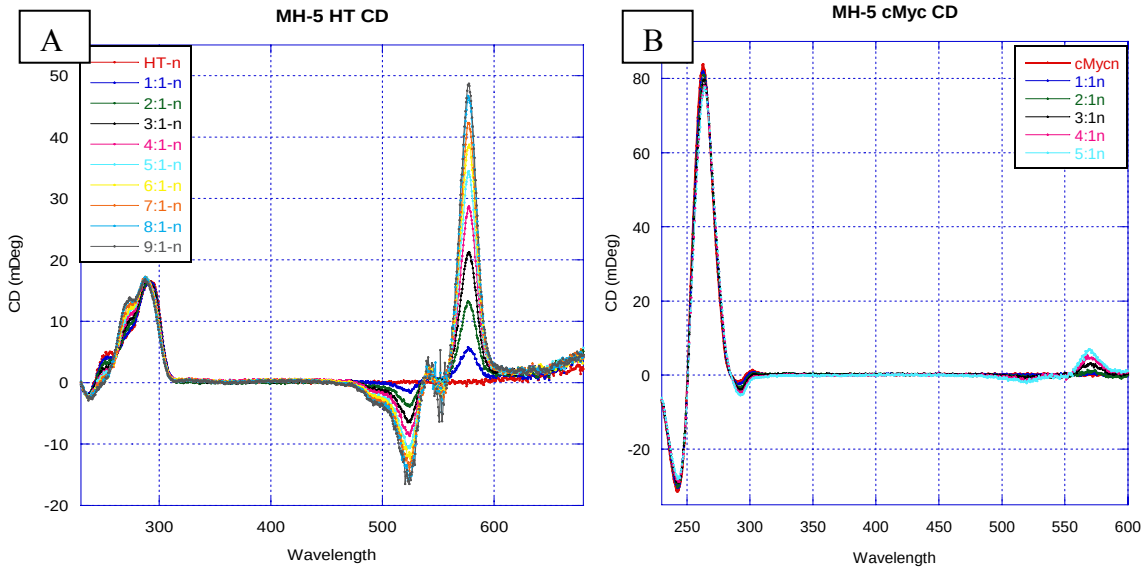

Figure 3.11 CD titrations done with 3 µM DNA on the Jasco J-810 Spectropolarimeter in Tris/K+ buffer. The solution is scanned from 230 nm to 700 nm at 25 ˚C with a scan rate of 50 nm/min, slit width of 1 nm, and a response time of 1 second. 3 µM of MH-5 was titrated for each scan. A) Titration of MH-5 into hTelo. B) Titration of MH-5 into *c-myc*.

Many of these compounds show great stabilization of the quadruplex motif in thermal melting data, and quadruplex specificity in SPR and ITC. Loop binding is the least specific mode of binding to quadruplex, so the compounds are most likely end stacking on both hTelo and c-*myc*. However, so much is still unknown about quadruplex binding that more experimentation is necessary to determine exact binding mode.

3.3.2 Pentamethine cyanine dyes

General structures of all pentamethine dyes are shown in Figure 3.12. These structures all maintain the same nitrogen substituent (trimethyl amine), but vary substituents on either the ring system, the linking methine, or both. These dyes are generally easier to handle; they are slightly less sticky to tubing and cell walls, while maintaining the quadruplex over duplex specificity seen with trimethine dyes due to the two methyl groups on the indolenes.

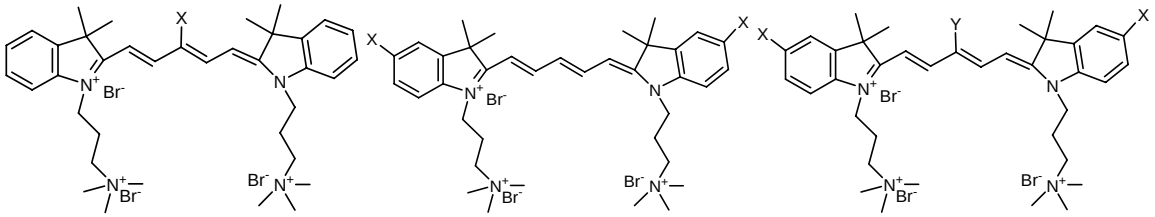

Figure 3.12 General structure of pentamethine mono- (left) di- (middle) and tri- (right) substituted dyes synthesized by Dr. Henary *et al* (Georgia State University, Atlanta, GA).

In general, pentamethine monohalogenated dyes show weaker binding than trimethine dihalogenated dyes based on the thermal melting data. The monobromo- and monochloro- dyes show similar stabilization at the 4:1 ratio (presumed saturation conditions) shown in Table 3.7, and thus do not follow the trend seen with the dihalogenated trimethine dyes. The bromo-dye most likely stacks more than the chloro- isomer, based on their increases at 6:1 ratios with the reverse true at lower ratios. As consistent with prior experiments, the carboxyl group on A-100 prevents binding. Only the bromo- isomer of pentamethine dihalogenated dyes has been synthesized, and it has a comparable quadruplex stabilization to the trimethine derivative. The size of the halogen substituents may allow necessary DNA to compound interactions to occur easier than with only hydrogens on the ring. The stabilization decreases for unsubstituted dyes as the linker lengthens (comparing MH-4 to E-46).

Table 3.7 Pentamethine mono- and di- substituted dyes thermal melting (ΔT_m) data (°C)

	Human Telomere				Duplex			
	1:1	**2:1**	**4:1**	**6:1**	**1:1**	**2:1**	**4:1**	**6:1**
E-46 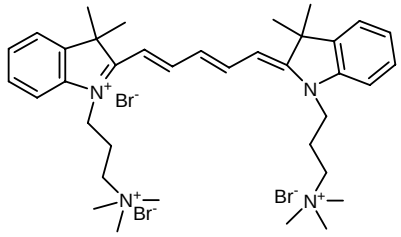	0.0	-0.4	-0.4	-3.8	-1.0	-0.9	0.0	-0.8
A-100 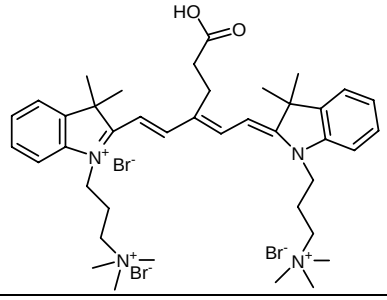	0.1	0.2	1.2	1.2				
A-C8 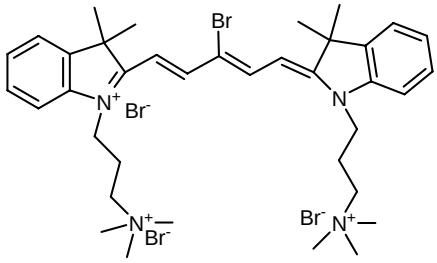	2.0	4.6	11.6	15.6	-0.0	-1.1	0.9	-0.2
A-20 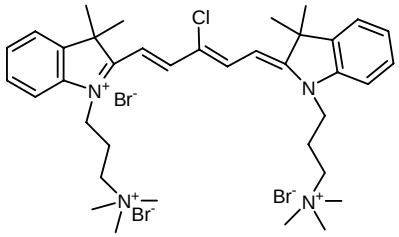	2.6	6.0	12.2	13.2	0	0.9	0.9	2.8

E-48 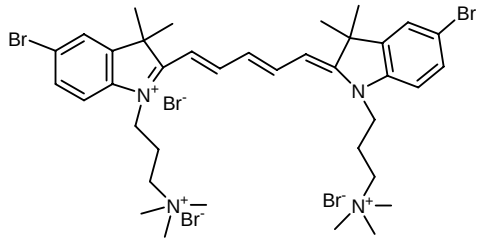	1.5	2.5	15.6	11.6	*	1.1	-0.7	0.0
*Experiment was too noisy to calculate accurate ΔT_m Note: Some compounds were not tested with duplex due to poor stabilization of quadruplex.								

SPR sensorgrams correlate well with thermal melting data, though data fitting is difficult with both hTelo tests, since the compounds do not bind strongly and have a weak binding site. SPR steady state response fits are shown in Figure 3.13. Thermodynamic data was also collected for A-C8 (Figure 3.14 with corresponding data in Table 3.8); again the stoichiometry differed, but is proven to bind preferentially to one binding site with a possible secondary binding site by mass spectrometry.

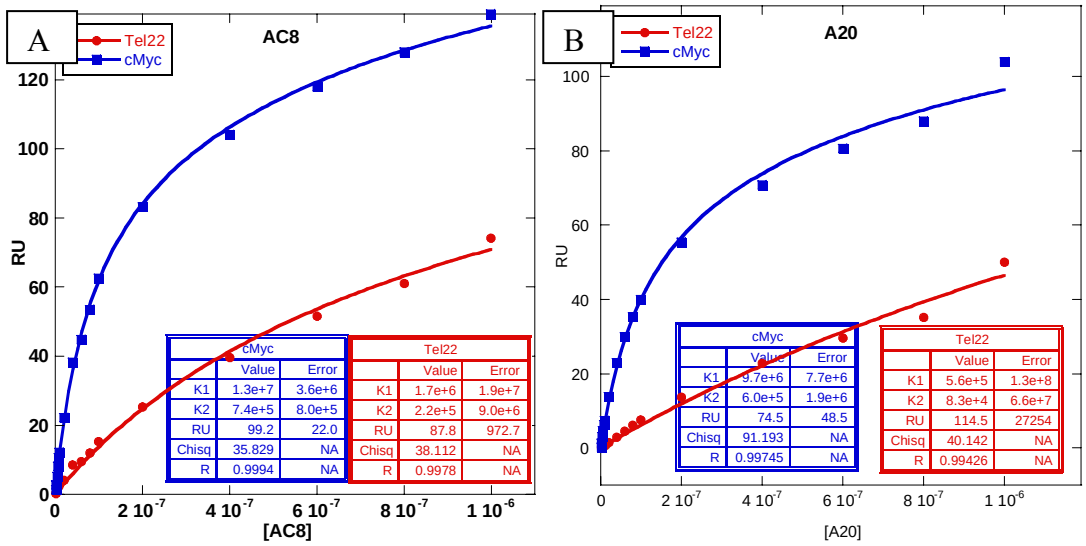

Figure 3.13 SPR steady state response fits for RHPS4 with c-*myc* and hTelo. Biotin labeled DNAs on chip were hTelo 22, c-*myc*19, and AATT hairpin. BIAcore 2000 optical biosensor system (GE Healthcare, Sweden) was used with HEPES buffer with .01% P20. Testing was performed using regeneration buffer 10 mM glycine at pH 2.5, 200 s injection time, 400 s dissociation time, a flow rate of 25 µL/min, and a temperature of 25 ˚C. A) A-C8 B)A-20. Experiments done in collaboration with Dr. Rupesh Nanjuda.

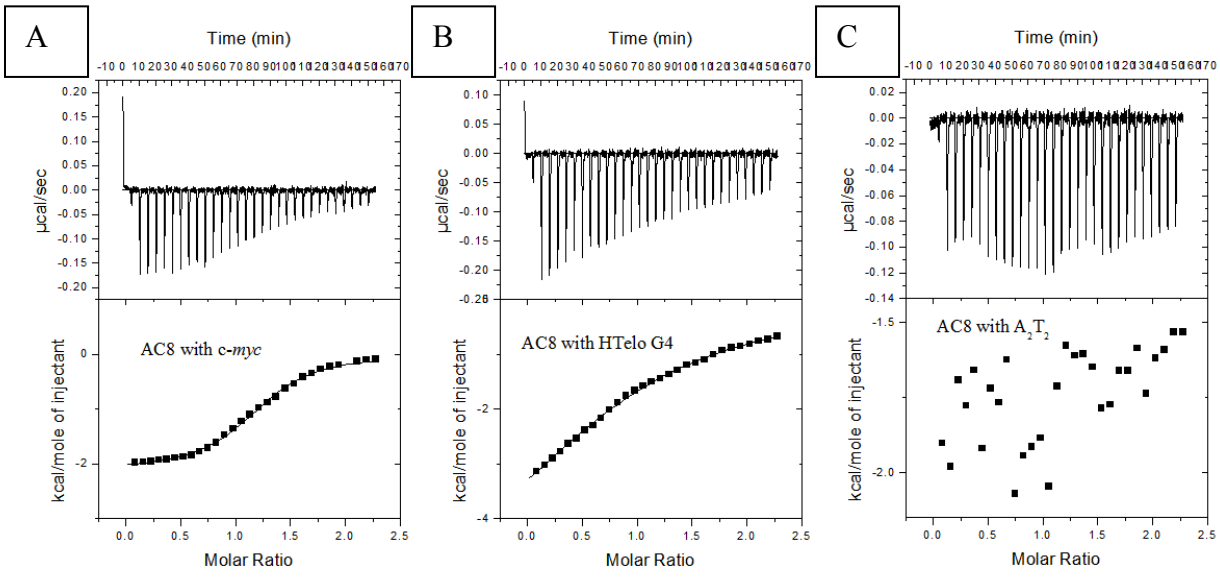

Figure 3.14 ITC Titrations of 0.2 mM A-C8 into 0.02 mM DNA. VPC-ITC with VPViewer 2000 software was used. Reference cell and solutions contained TRIS/K^+ buffer. 30 injections were measured at 25 ˚C with reference power of 1 µcal/s and 300 s spacing time. A) c-*myc* B) hTelo C) AATT duplex. Experiments done by Nancy Kilpatrick.

Table 3.8 Thermodynamics data for A-C8 binding

Oligomer	Stoichiometry	K (M^{-1})	Δ H (cal/mol)	Δ S (cal/mol C^o)	Δ G (cal/mol)
c-*myc*	1.22 ± 0.01	8.02E+05	-2100 ± 20	20	-8045.32
hTelo	1.02 ± 0.02	5.57E+04	-6100 ± 200	1.15	-6466.94
A_2T_2	No binding				

Fluorescence again confirms preference to c-*myc* over hTelo with an enormous increase in c-*myc* titrations and only a moderate increase with hTelo. A-20 fluorescence titrations are shown in Figure 3.15.

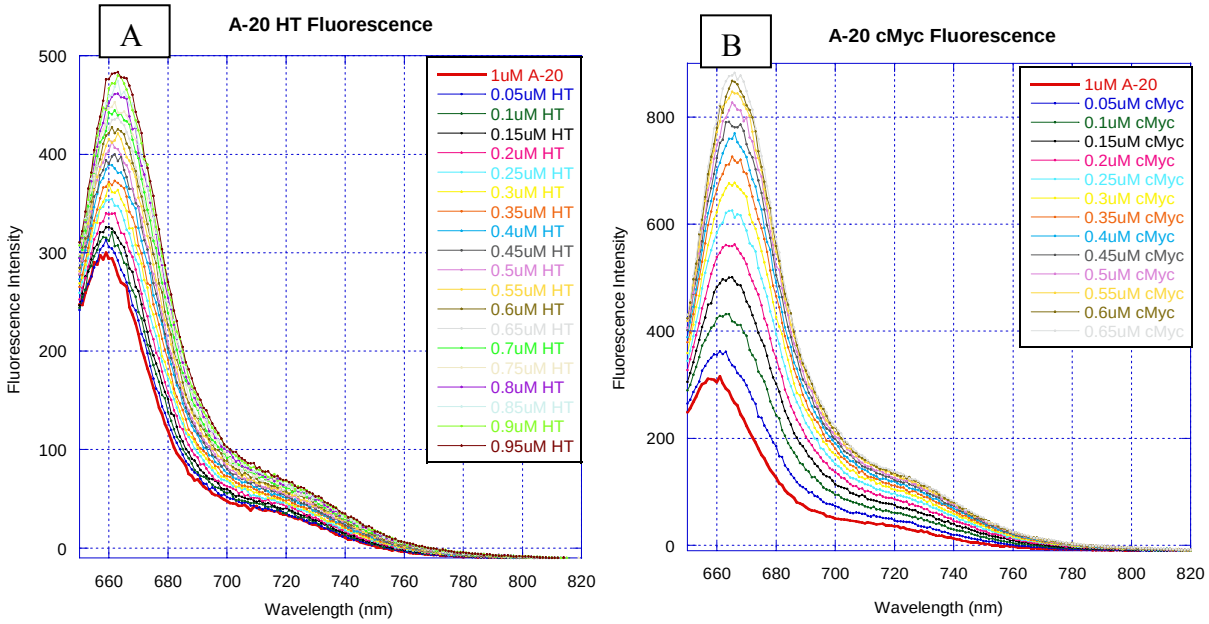

Figure 3.15 Results of fluorescent titration on Varian Cary Eclipse (Walnut Creek, CA) in TRIS/K^+ buffer. Slit widths were 5 nm (ex) and 5 nm (em). λ_{ex} was 640.0 nm and λ_{em} was taken from 650 nm to 820 nm. A) 1µM A-20 titrated with 0.05µM increments of hTelo. B) 1µM A-20 titrated with 0.05µM increments of *c-myc*. Slit widths were 5 nm (ex) and 5 nm (em).

CD scans are taken to determine binding mode, but as with trimethine dyes, no significant changes to the DNA region are observed. Monohalogenated dyes seem to be slower at binding as a slight change from hybrid to antiparallel motif is observed when a prepared sample was allowed to sit for approximately two hours. However, no induced CD is observed and both DNA sequences show less change in DNA region CD spectra with compound titrated into solution, seen in Figure 3.16.

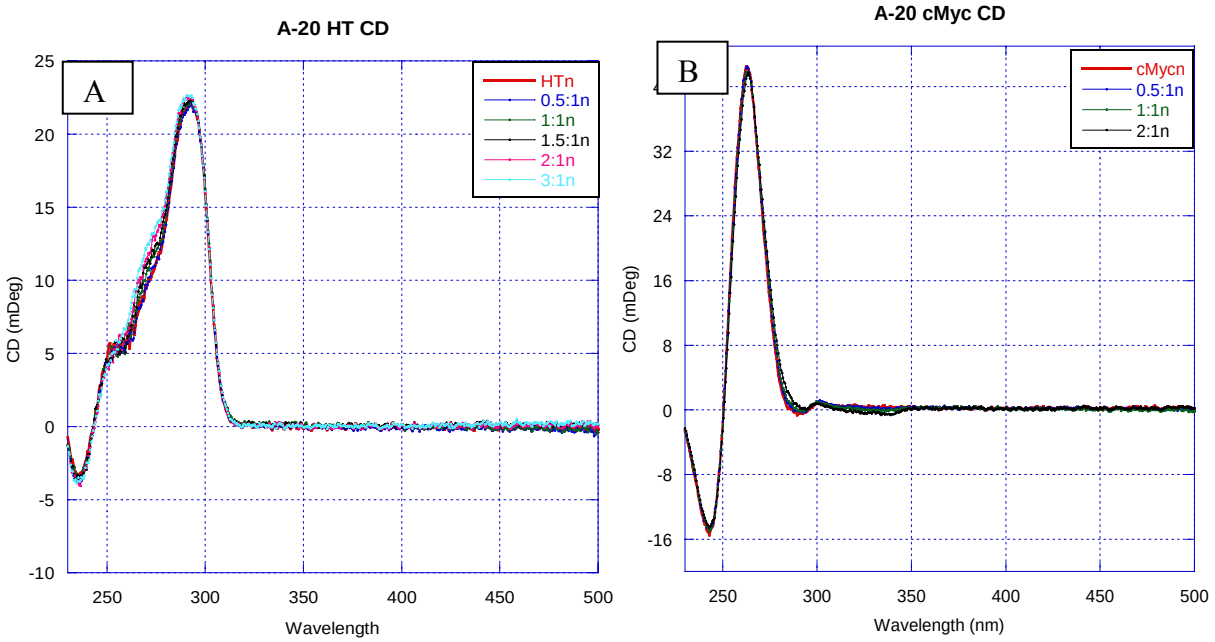

Figure 3.16 CD titrations done with 3 µM DNA on the Jasco J-810 Spectropolarimeter in Tris/K+ buffer. The solution is scanned from 230 nm to 700 nm at 25 ˚C with a scan rate of 50 nm/min, slit width of 1 nm, and a response time of 1 second. 3 µM of MH-5 was titrated for each scan. A) Titration of A-20 into hTelo. B) Titration of A-20 into *c-myc*.

Mass spectrometry is done with the strongest binding monohalogenated cyanine dye- A-C8, as strong binding compounds are required to remain bound in the charged gas state needed for electrospray ionization. The 1:1 peak is favored, as seen with trimethine dyes, but a 2:1 peak

forms at lower ratios of compound to DNA. As seen in Figure 3.17, the 2:1 peak of c-*myc* with A-C8 requires less compound to form than the 2:1 peak with MH-5. This peak can only be seen at the 4:1 ratio with MH-5, but can be seen at the 2:1 ratio with A-C8.

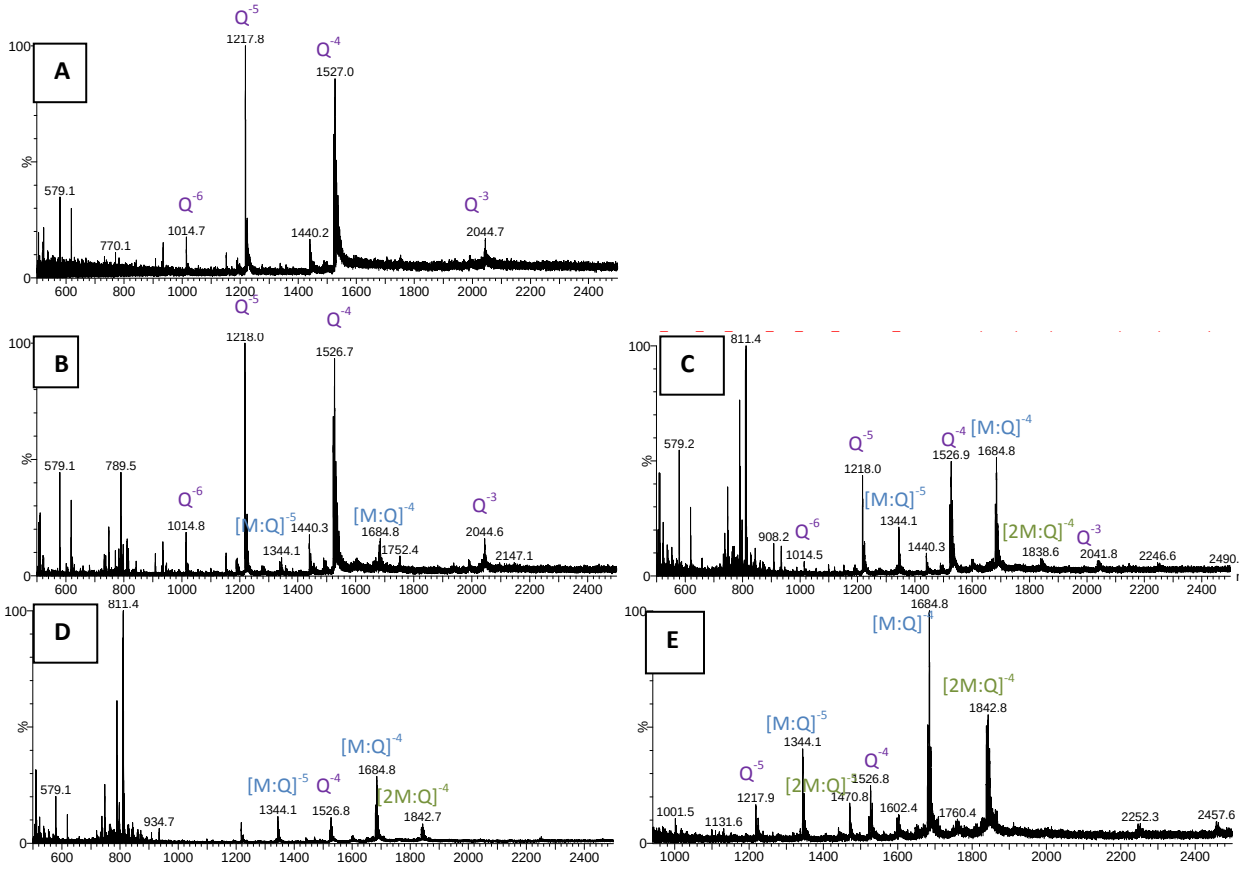

Figure 3.17 Electrospray ionization mass spectrometry results from Waters Micromass Q-TOF micro in ammonium acetate buffer. Spectra taken in negative mode with voltage of 2500 mV. A-C8 with c-*myc* mass spectrum with 10% methanol. A) 10µM c-*myc* B) 1:1 ratio C) 2:1 ratio D) 4:1 ratio E) 6:1 ratio.

Pentamethine trisubstituted compounds prove to be sticky to tubing and cell walls, but maintain previously established trends: the two methyl groups prevent duplex binding, and the sulfonate groups on A-21 minimize quadruplex binding. Thermal melting data (Table 3.9) reveals a possible indication of where on the compound DNA interactions may occur. If the ring halogens remain constant and the methine halogen is varied (in the case of A-150 to A-149, A-148 to A-146, and A-161 to A-160), a methine-linked bromine consistently raises the stabilization of DNA compared to compounds with methine-linked chlorine. When the ring halogens are varied and the methine halogen remains the same (in the case of A-150 to A-148 and A-161, and A-149 to A-146 and A-160), no trend can be recognized. Therefore, based on the saturation at 4:1 ΔT_m values, the methine-linked halogen is the primary cause of stabilization of quadruplex DNA. The compound must orient itself in a way that allows this halogen to interact with the bases along the groove or on the end, or the quadruplex-stabilizing cation, depending on how the compounds bind.

Table 3.9 Pentamethine trisubstituted dyes thermal melting (ΔT_m) data (°C)

	Human Telomere				Duplex			
(X-Y-Z)	**1:1**	**2:1**	**4:1**	**6:1**	**1:1**	**2:1**	**4:1**	**6:1**
A-21 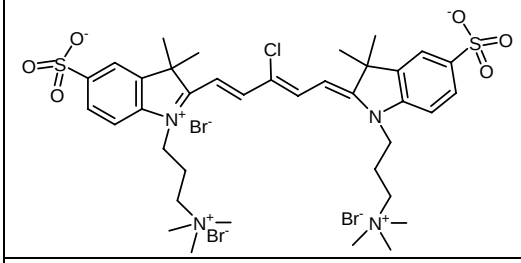	0.0	0.1	-0.4	0.2				
A-150 (Br-Br-Br) 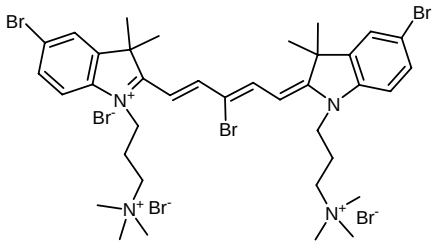	3.0	6.7	17.7	20.2	2.0	1.2	1.2	1.2
A-149 (Br-Cl-Br) 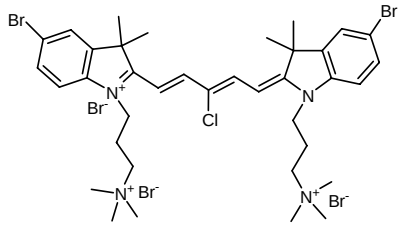	2.6	4.6	10.2	*				
A-148 (Cl-Br-Cl) 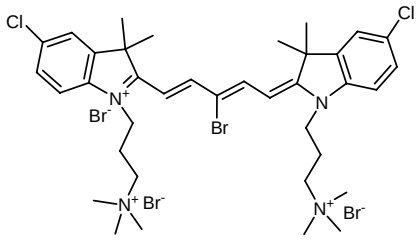	3.1	8.6	14.8	*				

A-146 (Cl-Cl-Cl) 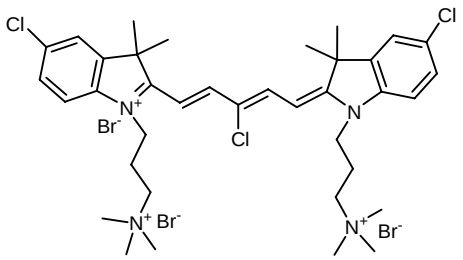	*	11.0	12.0	16.1	-1.0	0.1	-0.8	2.3
A-161 (I-Br-I) 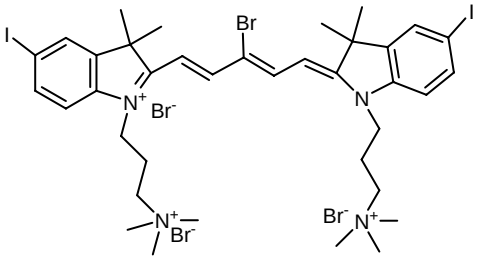	4.1	9.2	16.2	21.7				
A-160 (I-Cl-I) 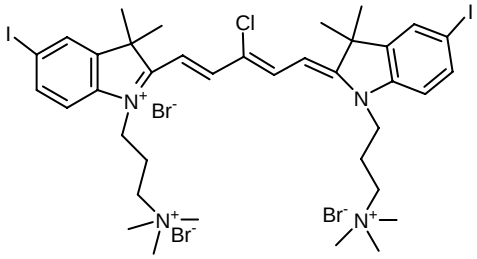	1.0	5.2	11.7	17.8				
(Error is ± 1 ˚C)								

When these compounds are tested with SPR, some of the binding affinities (primarily that of A-150) are found to be somewhat erratic and do not always correlate with the thermal melting data. Shown in the SPR steady state response fits in Figure 3.18, some of the compounds seem to be too sticky to tubing to test accurately or are merely weak binding compounds. To resolve this difference, a temperature controlled fluorescence experiment and a solvent variant absorbance experiment are done. A-150 has the highest discrepancy, so it is titrated with hTelo at 25 °C and 45 °C as shown in Figure 3.19.

Dimethyl sulfoxide (DMSO) is known to decrease self stacking in solution, so A-150 was tested with UV-Vis absorbance in three solutions: 100% Tris/K^+ buffer, 25% DMSO in buffer, and 50% DMSO in buffer (Figure 3.20). The absorbance intensity is expected to increase with more DMSO if stacking occurs. There was only a slight increase in absorbance as the percent DMSO increased, so the dye is not showing significant self stacking with no DNA present. Though the fluorescence emission decreases at a higher temperature, the fluorescence enhancement at the higher temperature is far greater than at room temperature. At higher temperatures, the compound is less likely to interact with the cell walls and tubing. Thermal melting analysis allows for this, but SPR is done at room temperature. The increased fluorescent enhancement indicates that the compound binds better at higher temperatures when aggregation is at a minimum, and temperature differences must be the cause of the discrepancy between SPR and ΔT_m values. Other room temperature fluorescent enhancements are shown in Table 3.10: they show no trends except confirmation that the preferences toward c-*myc* seen in SPR sensorgrams are accurate.

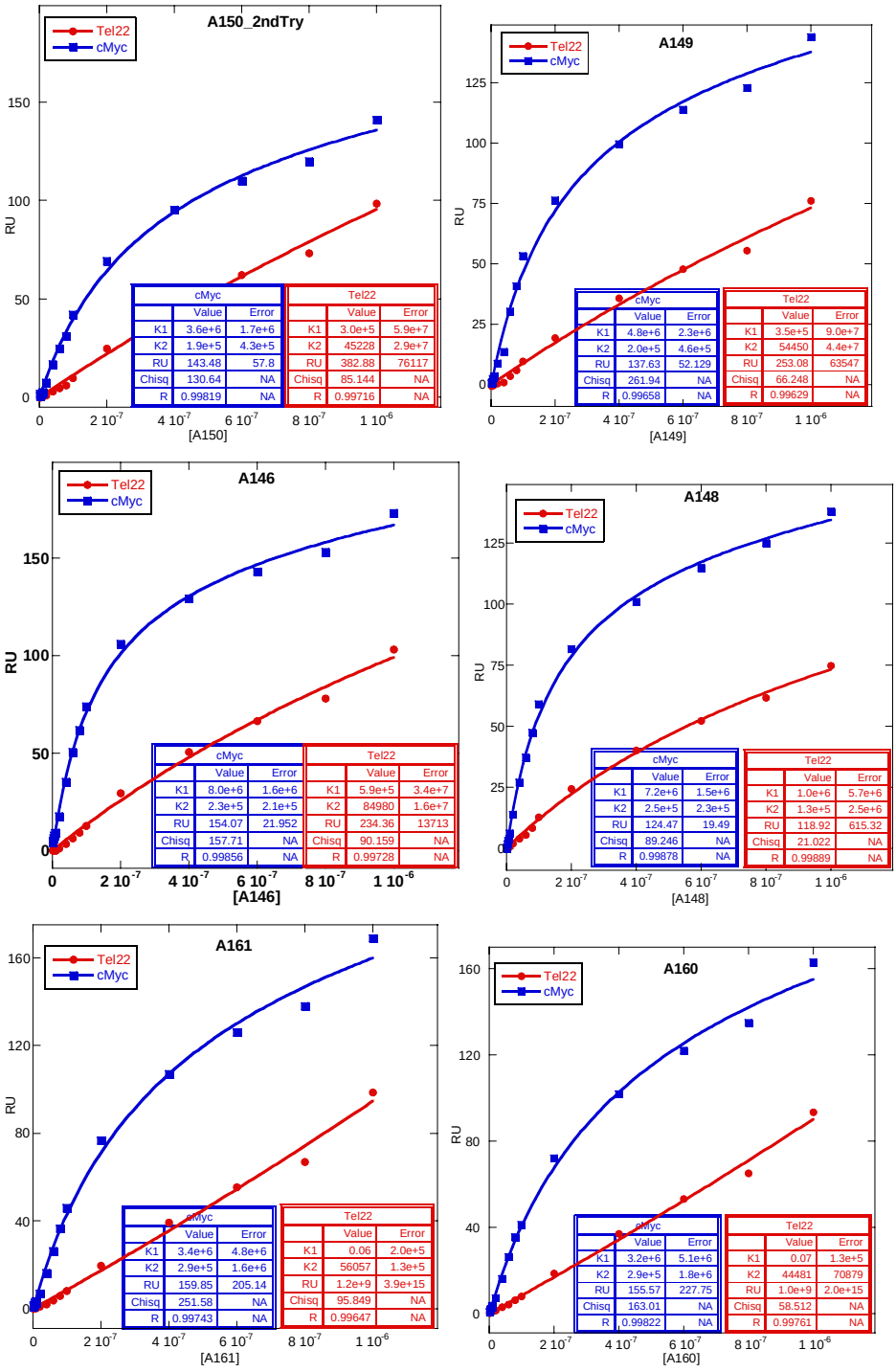

Figure 3.18 SPR steady state response fits for pentamethine dyes with c-*myc* and hTelo. Biotin labeled DNAs on chip were hTelo 22, c-*myc*19, and AATT hairpin. BIAcore 2000 optical biosensor system (GE Healthcare, Sweden) was used with HEPES buffer with .01% P20. Testing was performed using regeneration buffer 10 mM glycine at pH 2.5, 200 s injection time, 400 s dissociation time, a flow rate of 25 µL/min, and a temperature of 25 ˚C. Experiment done in collaboration with Dr. Rupesh Nanjuda.

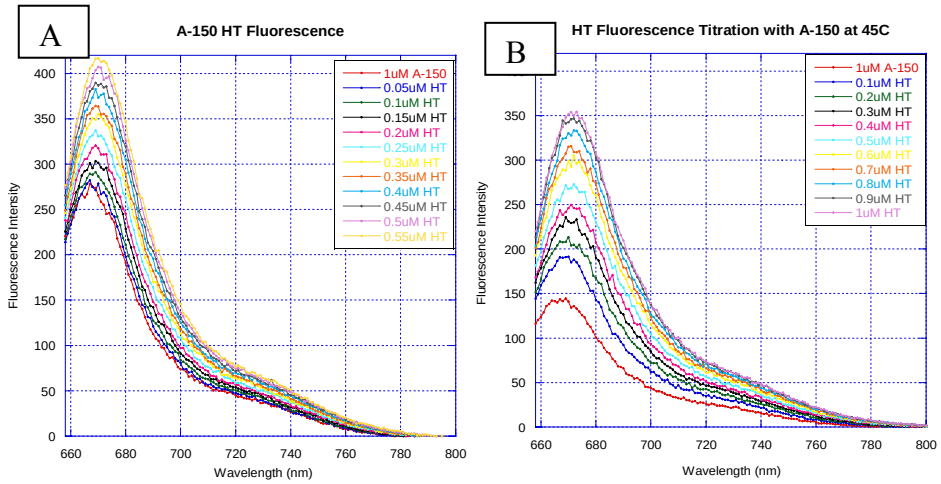

Figure 3.19 Results of fluorescent titration on Varian Cary Eclipse (Walnut Creek, CA) in TRIS/K^+ buffer. Slit widths were 5 nm (ex) and 5 nm (em). λ_{ex} was 650.0 nm and λ_{em} was taken from 658 nm to 800 nm. hTelo DNA titrated into A-150 at varying temperatures. A) 25˚C, fluorescent enhancement of 1.57 B) 45˚C, fluorescent enhancement of 2.64.

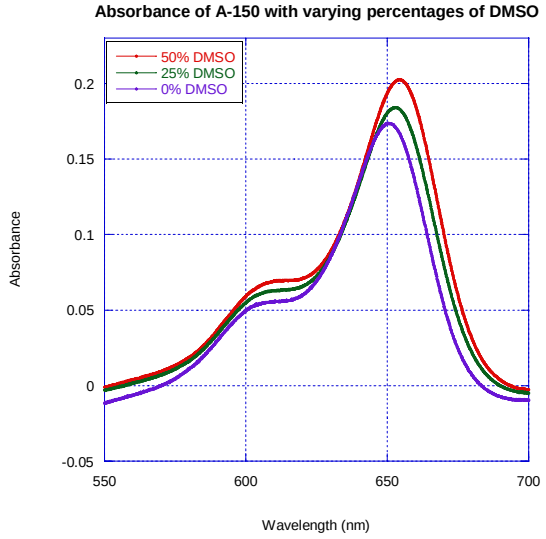

Figure 3.20 UV-Vis absorbance scans on Varian Cary 300 Bio Spectrophotometer (Walnut Creek, CA) of 1 µM A-150 in TRIS/K^+ buffer with v/v DMSO varying from 0% to 50%. Scanned 800 nm to 200 nm at a rate of 60 nm/min with a slit width of 2 nm.

Table 3.10 Pentamethine trihalogenated fluorescent enhancement ($F_{saturation}/F_{compound}$)

	HT	c-*myc*
A-21		1.0
A-146	1.8	2.2
A-148	1.7	2.0
A-149	1.8	2.2
A-150	1.6	2.4

Thermodynamic data from ITC is done at room temperature, but A-148 and A-150 are determined to have similar binding affinities as well as similar enthalpies, entropies, and Gibbs free energies when binding to c-*myc*. Shown in Figure 3.21 with corresponding data in Table 3.11, both compounds bind to c-*myc*, show weak (unable to fit) binding to hTelo, and do not bind to the tested duplex sequence.

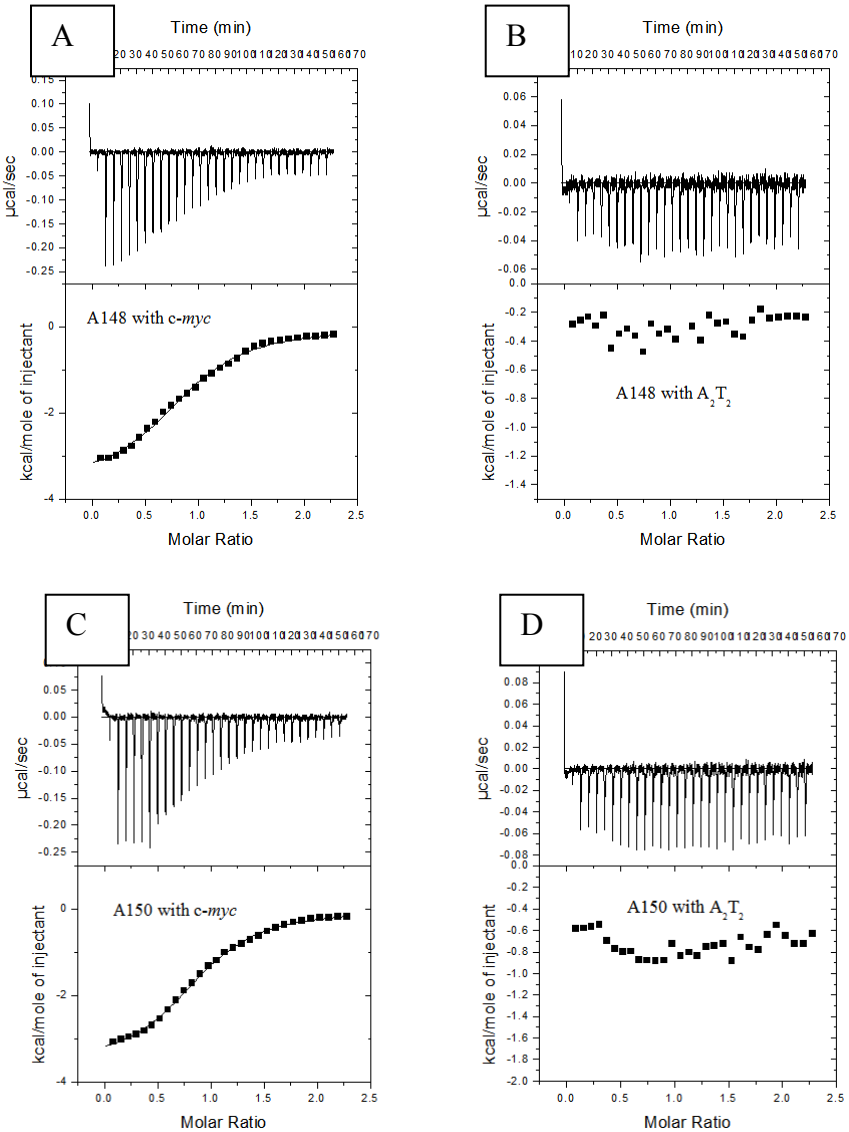

Figure 3.21 ITC Titrations of 0.2 mM compound into 0.02mM DNA. VPC-ITC with VPViewer 2000 software was used. Reference cell and solutions contained TRIS/K^+ buffer. 30 injections were measured at 25 ˚C with reference power of 1 µcal/s and 300 s spacing time. A) A-148 with c-*myc* B) A-148 with AATT duplex C) A-150 with c-*myc* D) A-150 with AATT. Experiments done by Nancy Kilpatrick.

Table 3.11 Thermodynamic data for A-148 and A-150 binding with c-*myc* (note both compounds showed weak binding with hTelo and no binding to AATT: data was unable to be fit)

Compound	Stoichiometry	K (M^{-1})	Δ H (cal/mol)	Δ S (cal/mol C^o)	Δ G (cal/mol)
A-148	0.91 ± 0.01	3.35E+05	-3670 ± 70	13.0	-7528.7
A-150	0.91 ± 0.01	3.97E+05	-3600 ± 40	13.5	-7629.2

Mass spectrometry for A-148 (Figure 3.22) and A-150 (Figure 3.23) show similar results to those seen with pentamethine monohalogenated compounds: the 1:1 peak is the favored binding ratio, and the 2:1 binding ratio is seen at a 2:1 solution ratio of compound to DNA. The unbound quadruplex peaks seem to be larger at higher compound to DNA ratios than with monohalogenated dyes. This may be due to the compounds' propensity to stack in solution; a large compound only peak is present at low m/z ratios, and increases at high compound concentrations. Therefore, at room temperature in the ESI instrument, the compound may be leaving more free DNA than it would at higher temperatures.

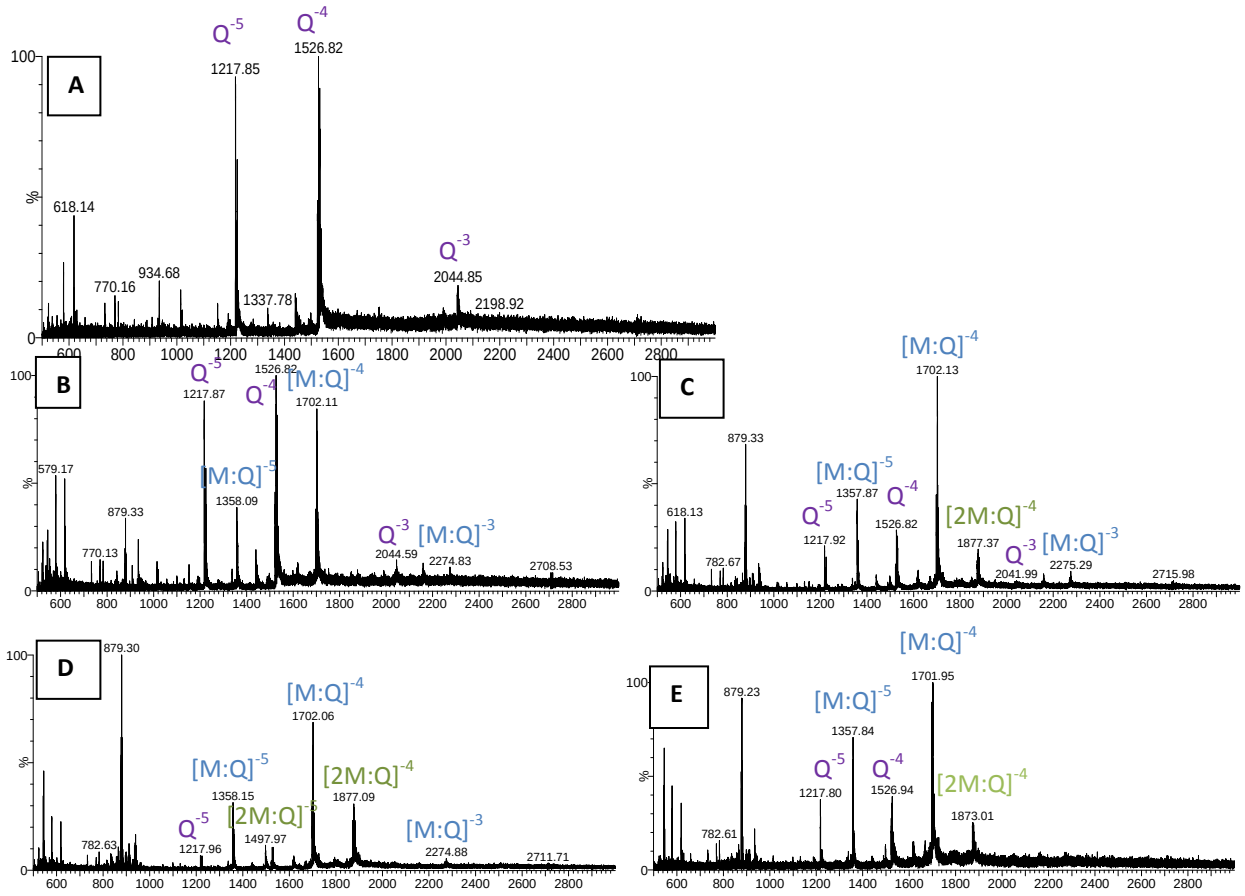

Figure 3.22 Electrospray Ionization mass spectrometry results from Waters Micromass Q-TOF micro in ammonium acetate buffer. Spectra taken in negative mode with voltage of 2500 mV. A-148 with c-*myc* mass spectrum with 10% methanol. A) 10 µM c-*myc* B) 1:1 ratio C) 2:1 ratio D) 4:1 ratio E) 6:1 ratio.

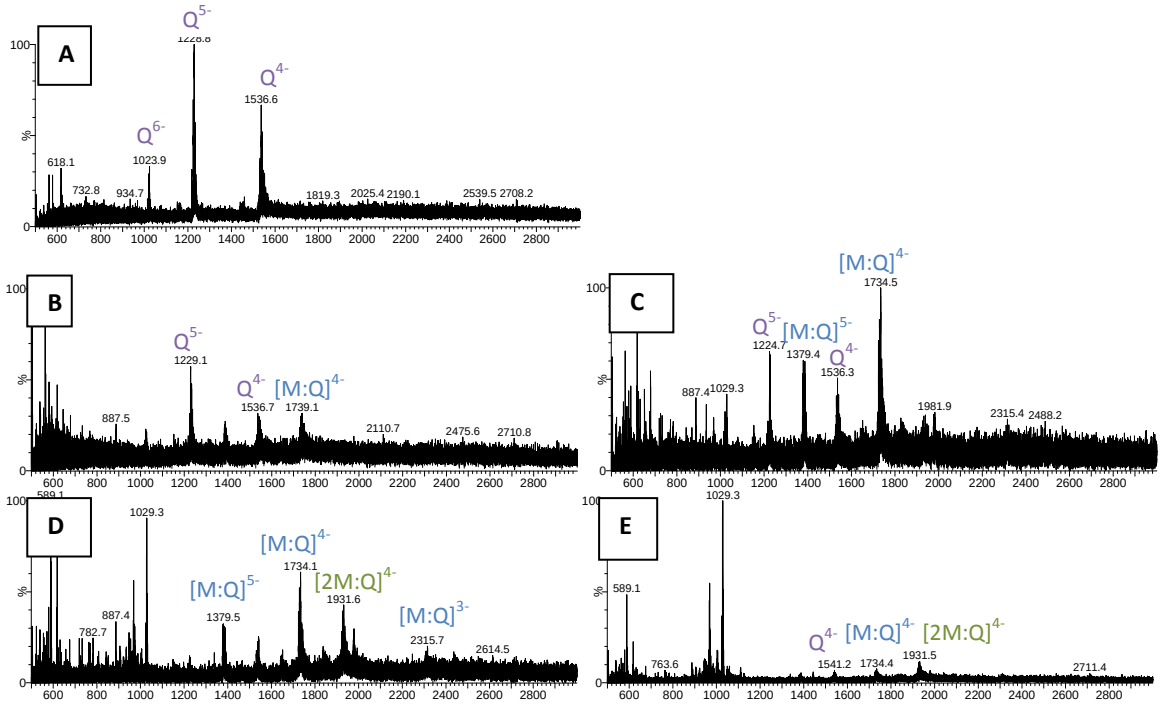

Figure 3.23 Electrospray Ionization mass spectrometry results from Waters Micromass Q-TOF micro in ammonium acetate buffer. Spectra taken in negative mode with voltage of 2500 mV. A-150 with c-*myc* mass spectrum with 10% methanol. A) 10 µM c-*myc* B) 1:1 ratio C) 2:1 ratio D) 4:1 ratio E) 6:1 ratio.

Chapter 4

Conclusions and Biological Implications

The results shown in this thesis provide suggestions to particular trends of chemical properties that assist in optimizing the process of developing compounds to bind specifically to quadruplex over duplex DNA. Clearly, compounds with negative charges (or overall charge of less than +3) prove to be poor binding compounds to all DNAs. Based on the benzothiozole cyanine dye results, the two methyl groups on the indolene block duplex binding. The benzothiozole rings lay in the minor groove of duplex DNA as sulfur interacts with the nucleotide bases and the positive ring nitrogen interacts with the phosphate backbone. The methyl groups prohibit interactions in the groove, but maintain the conjugation required to bind to the quadruplex DNA, probably in an end-stacking mode. In both benzothiozole and indolene cyanine dye complexes, binding affinity and stabilization is dependent on length and the ability for the compound to fit the shape of the quadruplex. Hydrophobic substituents replacing positively charged groups weakens binding due to their hydrophobicity and lessened polar interactions. Trimethine dihalogenated dyes form a trend in binding affinity and stabilization: the larger halogen on the ring systems yields stronger binding. No specific trends can be seen for the two pentamethine monohalogenated compounds, but the pentamethine trihalogenated compounds indicate a trend based on the central methine-linked halogen: binding is preferred with a smaller halogen on the linker. The compounds synthesized thus far only contain bromine and chlorine in this linker, but bromine-containing linkers seem to stabilize quadruplex DNA better than those with chlorine. When comparing pentamethine dyes with varying numbers of halogens, there is a clear increase in stabilization of hTelo with additional bromines, shown in Table 4.1.

Table 4.1 Thermal melting data (ΔT_m) of pentamethine cyanine dyes with hTelo (°C)

	1:1	2:1	4:1	6:1
E-46 (0 Br) 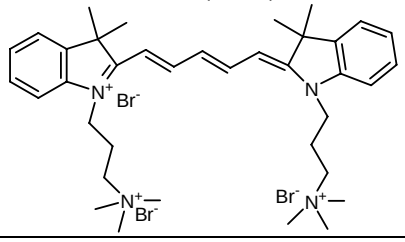	0.0	-0.4	-0.4	-3.8
A-C8 (1 Br) 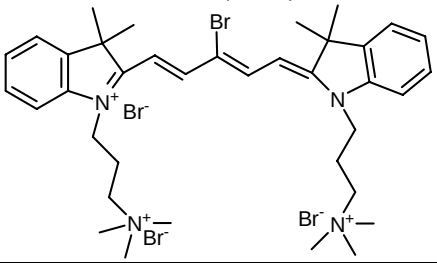	2.0	4.6	11.6	15.6
E-48 (2 Br) 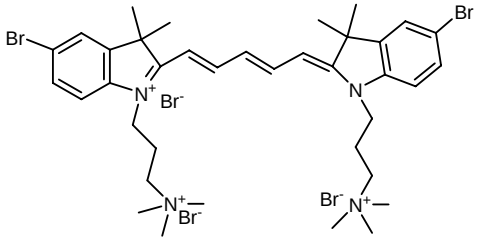	1.5	2.5	15.6	11.6
A-150 (3 Br) 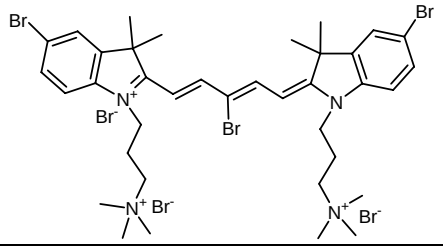	3.0	6.7	17.7	20.2
(Error is ± 1 ˚C)				

Thermodynamic comparisons of the tested compounds (Figure 4.1) show that MH-5 has the best Gibbs free energy for binding, and the trihalogenated dyes (A-148 and A-150) have the worst energetics. Entropic costs are approximately similar among all tested compounds, but the pentamethine monobromine dye A-C8 seems to have the worst enthalpy.

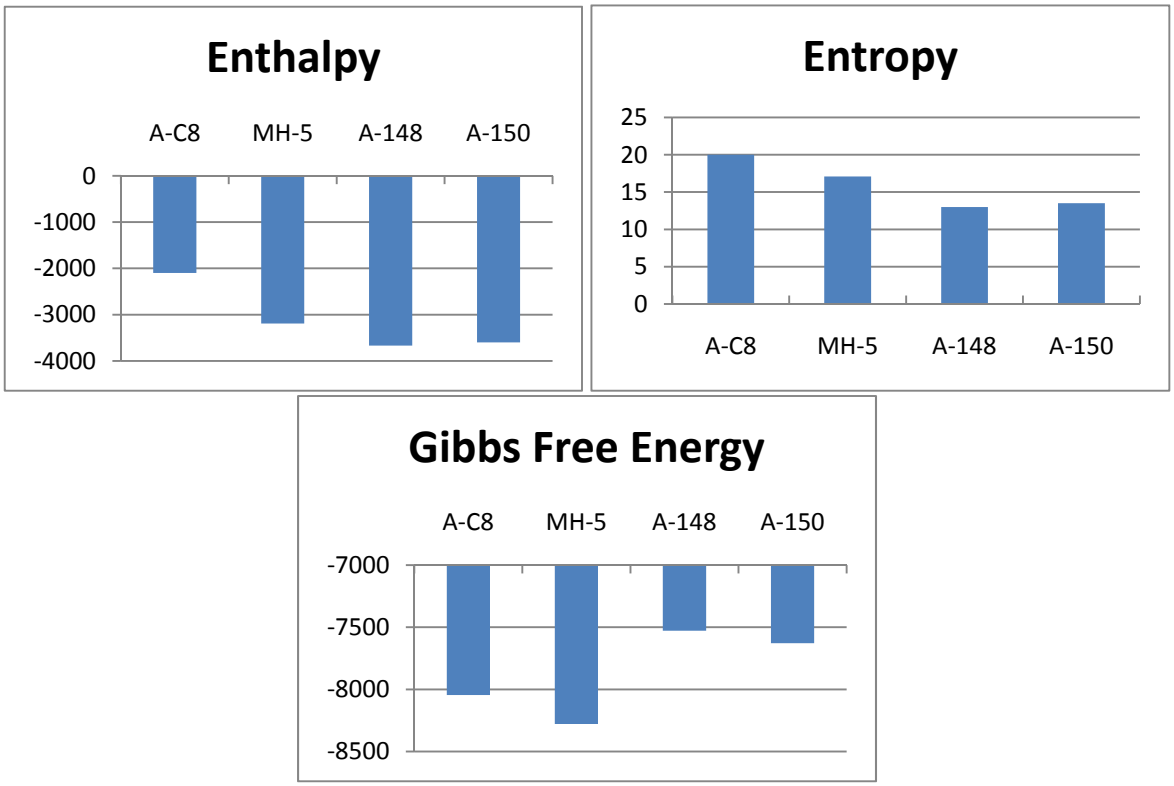

Figure 4.1 Graphs comparing thermodynamic data of all ITC tested compounds with c-*myc*.

In general, CD titrations show minimal change in the DNA region, indicating loop binding or end stacking. The induced CD seen in the compound region of the trimethine dihalogenated dyes is unique to that family of compounds. The trimethine nonsubstituted (MH-4) and the pentamethine disubstituted (E-48) cyanine dyes both show no induced CD in the compound regions. Additionally, the compound-only CD titration shows no induced CD, so these dyes must stack on the quadruplex in a unique way. The accuracy of NMR and crystallographic studies of quadruplex DNA is still highly debated, but these studies would be the most beneficial to understanding the unique binding of these trimethine symmetric indolene dyes.

Although only speculations about the DNA quadruplex binding mode can be made about these cyanine dye derivatives, one thing is clear; UV-Vis thermal melting, fluorescence, SPR,

and ITC experimental methods support binding specifically to *c-myc* parallel quadruplex over human telomere hybrid quadruplex, and to both quadruplex sequences over duplex DNA. This sequence specificity is rarely seen in other compounds and is deserving of further investigation. These particular compounds may not be future cancer treatment alternatives, but they suggest possible design directions. However, *in-vivo* experiments at Harvard Medical School have proved that these compounds are minimally toxic [unpublished results]. They show that many compounds get into specific cells: the dibromo trimethine dye (MH-5) shows specificity for liver, spleen, and small intestine cells, shown in Figure 4.2, and the dibromomonochloro pentamethine dye (A-148) even gets past the blood-brain barrier, shown in Figure 4.3.

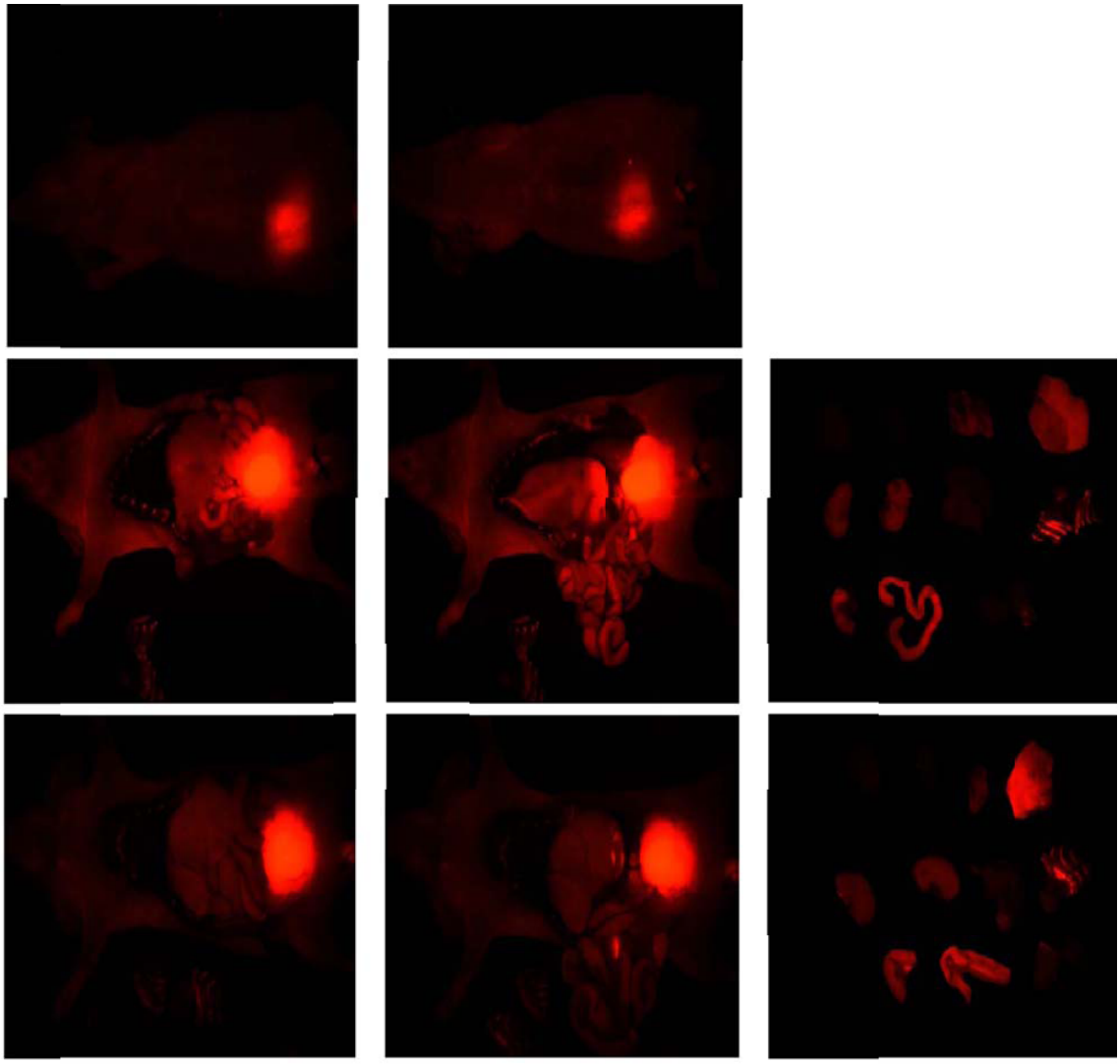

Figure 4.2 Dissection of mouse 4 hs after intravenous injection of 5 nmol MH-5. Fluorescent imaging done with 558 λ_{ex} and 578 λ_{em}, filter 525/560 LP. Figure shows dye localization in liver and bladder. Image from Dr. Frangioni Laboratory (Beth Israel Deaconess Medical Center) in collaboration with Dr. Maged Henary (Georgia State University).

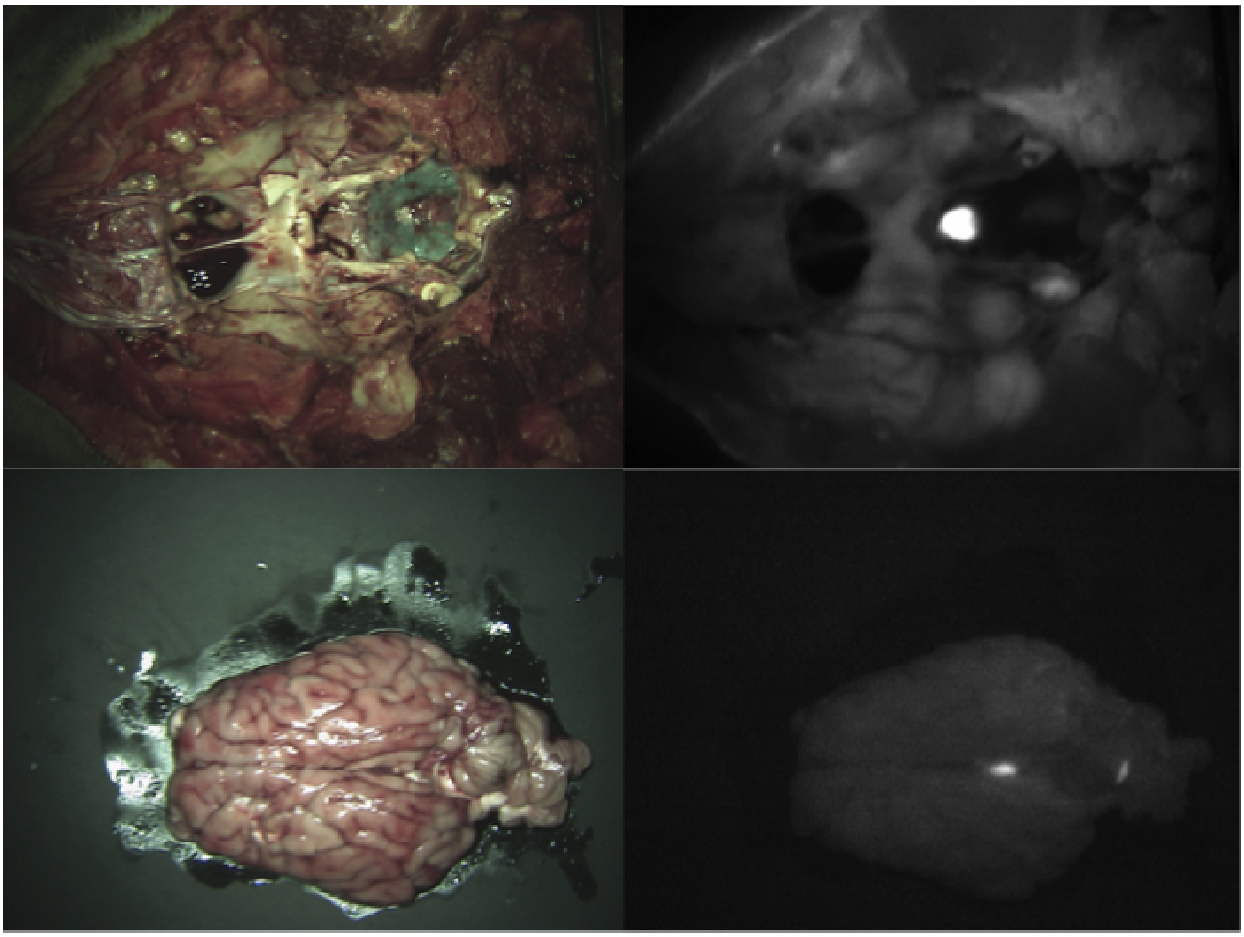

Figure 4.3 Pig brain after injection of A-148. Figure shows dye localization at the anterior side of the corpus callosum, in the pons. Image from Dr. Frangioni Laboratory (Beth Israel Deaconess Medical Center) in collaboration with Dr. Maged Henary (Georgia State University).

If a binding mode is to be proposed when comparing all cyanine dye derivatives in this study, it seems that the successful dyes end stack, using π-π bonds as the primary interaction. Collie *et al*. propose that two acridine-based compounds bind as dimer end stackers, with both acridines laying on a single tetrad (PDB file 3MIJ)[47]. This does not seem to be an appropriate binding model for cyanine dye derivatives, as a single binding site is clearly preferred. Additionally, binding is dependent on the halogen substituents, which could not fit in his proposed structure. Instead, these particular compounds may end stack as Drewe et al. propose

for their diarylureas:[42] compounds π-π stacking with two guanines in the terminal tetrad, and nonconjugated sidechains interacting with the loops. It seems that based on the length dependence, trimethine dyes fit better, which minimize the steric strain, allowing π-π interactions to form easily. The halogens on trimethine dyes may fit easily in two of the grooves, explaining the induced CD, whereas the pentamethine halogens are too far away from the grooves to alter the CD pattern. The other two grooves are most likely occupied by the trimethyl amine substituent. They would readily interact with the negative backbone, stabilizing the quadruplex structure, and explaining the large ΔT_m values.

These symmetric indolene cyanine dyes will continue to be designed to improve *in-vivo* successes to lead to better cancer treatments. These compounds can also help us understand quadruplex DNA and what compounds favor which structural motifs. These compounds' high binding specificity over duplex DNA and specificity towards parallel over hybrid may lead to a better understanding of quadruplex DNA. In turn this information may hopefully lead to a new paradigm to design more effective compounds for cancer-detecting dyes or anti-cancer treatments.

Chapter 5

References

1. Arya DP, Willis B. "Reaching into the Major Groove of B-DNA: Synthesis and Nucleic Acid Binding of a Neomycin-Hoechst 33258 Conjugate" *Journal of American Chemical Society*, **2003**, 125, 12398-12399.
2. Turner PR, Denny WA. "The Genome as a Drug Target: Sequence Specific Minor Groove Binding Ligands." *Current Drug Targets*, **2000**, 1, 1-14.
3. Potaman VN, Sinden RR. "DNA: Alternative Conformations and Biology" *DNA Conformation and Transcription,* Akashi Ohyama Ed. **2004**.
4. Neidle S, Schneider B, Berman HM. "Fundamentals of DNA and RNA Structure" *Structural Bioinformatics*, Second Ed. Co. John Wiley and Sons, Inc. **2009**.
5. Eritja R, Mergny JL, Montesarchio D, Spindler L, Webba da Silva M. "G-Quadruplex Nucleic Acids." *Journal of Nucleic Acids*, **2010**, 1-2.
6. Huppert JL. "Four-stranded nucleic acids: structure, function and targeting of G-quadruplexes." *Chemical Society Review*, **2008**, 37, 1375–1384.
7. Phan AT, Luu KN, Patel DJ. "Different loop arrangements of intramolecular human telomeric (3+1) G-quadruplexes in K+ solution." *Nucleic Acids Research*, **2006**, 34, 5715–5719.
8. Luu KN, Phan AT, Kuryavyi V, Lacroix L, Patel DJ. "Structure of the Human Telomere in K+ Solution: An Intramolecular (3 + 1) G-Quadruplex Scaffold." *Journal of American Chemical Society,* **2006**, 128, 9963-9970.
9. Xue Y, Kan ZY, Wang Q, Yao Y, Liu J, Hao YH, Tan Z. "Human Telomeric DNA Forms Parallel-Stranded Intramolecular G-Quadruplex in K+ Solution under Molecular Crowding Condition." *Journal of American Chemical Society*, **2007**, 129, 11185-11191.
10. Pradhan D, Hansen LH, Vester B, Petersen M. "Selection of G-Quadruplex Folding Topology with LNA-Modified Human Telomeric Sequences in K+ Solution" *Chemistry European Journal*, **2011**, 17, 405 – 2413.
11. Cang X, Sˇponer J, Cheatham III TE. "Explaining the varied glycosidic conformational, G-tract length and sequence preferences for anti-parallel G-quadruplexes" *Nucleic Acids Research,* **2011**, 39, 1–14.
12. Webba da Silva M, Trajkovski M. "Design of a G-Quadruplex Topology through Glycosidic Bond Angles" *Angew. Chemistry International Ed*., **2009,** 48, 9167 –9170.
13. Esposito V, Oliviero G, Pepe A, Virgilio A, Galeone A. "Studies on the Influence of Inversion of Polarity Sites on the dG residues glycosidic conformation in Quadruplex Structures" *Nucleic Acids Symposium Series No. 52,* **2008**, 177-178.
14. Gaynutdinov TI, Neumann RD, Panyutin IG. "Structural polymorphism of intramolecular quadruplex of human telomeric DNA: effect of cations, quadruplex-binding drugs and flanking sequences" *Nucleic Acids Research,* **2008**, 36, 4079–4087.
15. Haider SM, Neidle S. "A molecular model for drug binding to tandem repeats of telomeric G-quadruplexes." *Biochemical Society Annual Symposium No. 76,* **2009**, 583-588.
16. Ma H, Zhang M, Zhang D, Huang R, Zhao Y, Yang H, Liu Y, Weng X, Zhou Y, Deng M, Xu L, Zhou X. "Pyridyl-Substituted Corrole Isomers: Synthesis and their Regulation to G-quadruplex Structures" *Chemistry: An Asian Journal,* **2010**, 5, 114-122.
17. Garner TP, Williams HEL, Gluszyk KI, Roe S, Oldham NJ, Stevens MFG, Moses JE, Searle MS. "Selectivity of small molecule ligands for parallel and anti-parallel DNA G-quadruplex structures" *Journal of Organic & Biomolecular Chemistry*, **2009**, 7, 4194-4200.

18. Sparapani S, Haider SM, Doria F, Gunaratnam M, Neidle S. "Rational Design of Acridine-Based Ligands with Selectivity for Human Telomeric Quadruplexes." *Journal of American Chemical Society*, **2010**, 132, 12263-12272.
19. Debray J, Zeghida W, Jourdan M, Monchaud D, Dheu-Andries ML, Dumy P, Teulade-Fichou MP, Demeunynck M. "Synthesis and evaluation of fused bispyrimidinoacridines as novel pentacyclic analogues of quadruplex-binder BRACO-19" *Journal of Organic & Biomolecular Chemistry*, **2009**, 7, 5219–5228.
20. Babu B, Liu Y, Plaunt A, Riddering C, Ogilvie R, Westrate L, Davis R, Ferguson A, Mackay H, Rice T, Chavda S, Wilson WD, Lin S, Kiakos K, Hartley JA, Lee M. "Design, synthesis and DNA binding properties of orthogonally positioned diamino containing polyamide f-IPI" *Biochemical and Biophysical Research Communications*, **2011**, 404, 848-852.
21. White EW, Tanious F, Ismail MA, Reszka AP, Neidle S, Boykin DW, Wilson WD. "Structure-specific recognition of quadruplex DNA by organic cations: Influence of shape, substituents and charge" *Biophysical Chemistry*, **2007**, 126, 140–153.
22. Neidle S. "Human telomeric G-quadruplex: The current status of telomeric G-quadruplexes as therapeutic targets in human cancer." *FEBS Journal*, **2010**, 277, 1118–1125.
23. Neidle S, Parkinson G. "Telomere maintenance as a target for anticancer drug discovery" *Nature Reviews Drug Discovery*, **2002**, 1, 383-393.
24. Manet I, Manoli F, Zambelli B, Andreano G, Masi A, Cellai L, Monti S. "Affinity of the anthracycline antitumor drugs Doxorubicin and Sabarubicin for human telomeric G-quadruplex structures" *Journal of Physical Chemistry,* **2011**, 13, 540-541.
25. Bianco S, Musetti C, Waldeck A, Sparapani S, Seitz JD, Krapcho AP, Palumbo M, Sissi C. "Bis-phenanthroline derivatives as suitable scaffolds for effective G-quadruplex recognition" *Dalton Transactions*, **2010**, 39, 5833–5841.
26. Meyerson M. "Role of Telomerase in Normal and Cancer Cells" *Journal of Clinical Oncology,* **2000**, 18, 2626-2634.
27. Levens D. "You Don't Muck with MYC" *Genes Cancer*. **2010**, 1, 547–554.
28. Drygin D, Rice WG, Grummt I. "The RNA Polymerase I Transcription Machinery: An Emerging Target for the Treatment of Cancer" *Annual Review of Pharmacological Toxicology,* **2010**, 50, 131-156.
29. Fu YT, Keppler BR, Soares B, Jarstfer MB "BRACO19 analog dimers with improved inhibition of telomerase and hPot 1" *Journal of Bioorganic & Medicinal Chemistry*, **2009**, 17, 2030–2037.
30. Armitage B. "Cyanine Dye-DNA Interactions: Intercalation, Groove Binding, and Aggregation." *Topics of Current Chemistry,* **2005**, 253, 55-76.
31. Peng X, Wu T, Fan J, Wang J, Zhang S, Song F, Sun S. "An Effective Minor Groove Binder as a Red Fluorescent Marker for Live-Cell DNA Imaging and Quantification" *Angew. Chemistry International Ed.*, **2011**, 50, 1 – 5.
32. Stadler AL, Renikuntla BR, Yaron D, Fang AS, Armitage BA. "Substituent Effects on the Assembly of Helical Cyanine Dye Aggregates in the Minor Groove of a DNA Template" *Langmuir*, **2011**, 4, 1472-1479.
33. Li T, Wang E, Dong S. "Parallel G-Quadruplex-Specific Fluorescent Probe for Monitoring DNA Structural Changes and Label-Free Detection of Potassium Ion." *Journal of Analytical Chemistry,* **2010**, 82, 7576-7580.

34. Koripelly G, Meguellati K, Ladame S. "Dual Sensing of Hairpin and Quadruplex DNA Structures Using Multicolored Peptide Nucleic Acid Fluorescent Probes" *Bioconjugate Chemistry*, **2010**, 21, 2103–2109.
35. Shi C, Zhang C, Su Y, Cheng T. "Cyanine dyes in optical imaging of tumours" *The Lancet Oncology,* **2010**, 11, 815-816.
36. Lubitz, I, Zikich, D, Kotlyar, A. "Specific High-Affinity Binding of Thiazole Orange to Triplex and G-Quadruplex DNA" *Biochemistry*, **2010**, 49, 3567–3574.
37. Zhang C, Liu T, Su Y, Luo S, Zhu Y, Tan X, Fan S, Zhang L, Zhou Y, Cheng T, Shi C. "A near-infrared fluorescent heptamethine indocyanine dye with preferential tumor accumulation for in vivo imaging" *Biomaterials*, **2010**, 31, 6612-6617.
38. Meguellati K, Koripelly G, Ladame S. "DNA-Templated Synthesis of Trimethine Cyanine Dyes: A Versatile Fluorogenic Reaction for Sensing G-Quadruplex Formation" *Angew. Chemistry International Ed.*, **2010**, 49, 2738 –2742.
39. Yang Q, Xiang J, Yang S, Li Q, Zhou Q, Guan A, Zhang X, Zhang H, Tang Y, Xu G. "Verification of specific G-quadruplex structure by using a novel cyanine dye supramolecular assembly: II. The binding characterization with specific intramolecular G-quadruplex and the recognizing mechanism" *Nucleic Acids Research*, **2010**, 38, 1022–1033.
40. Denis Drygin *et al*, "Anticancer Activity of CX-3543: A Direct Inhibitor of rRNA Biogenesis" *Cancer Research*, **2009**, 69, 7653-7661.
41. Lim KW, Amrane S, Bouaziz S, Xu W, Mu Y, Patel DJ, Luu KN, Phan AT. "Structure of the human telomere in K+ solution: a stable basket type G-quadruplex with only two G-tetrad layers" *Journal of American Chemical Society,* **2009**, 12, 4301–4309.
42. Drewe WC, Nanjunda R, Gunaratnam M, Beltran M, Parkinson GN, Reszka AP, Wilson WD, Neidle S. "Rational Design of Substituted Diarylureas: A Scaffold for Binding to G-Quadruplex Motifs" *Journal of Medical Chemistry,* **2008**, *51,* 7751–7767.
43. Rosu F, Gabelica V, Poncelet H, Pauw ED. "Tetramolecular G-quadruplex formation pathways studied by electrospray mass spectrometry" *Nucleic Acids Research*, **2010**, 38, 5217-5225.
44. Podbevsˇek P, Hud NV, Plavec J. "NMR evaluation of ammonium ion movement within a unimolecular G-quadruplex in solution" *Nucleic Acids Research*, **2007**, 35, 2554–2563.
45. Pagano B, Mattia CA, Giancola C. "Applications of Isothermal Titration Calorimetry in Biophysical Studies of G-quadruplexes" *International Journal of Molecular Science,* **2009**, 10, 2935-2957.
46. Yang Q, Xiang JF, Yang S, Li Q, Zhou Q, Guan A, Li L, Zhang Y, Zhang X, Zhang H, Tang Y, Xu G. "Verification of Intramolecular Hybrid/Parallel G-Quadruplex Structure under Physiological Conditions Using Novel Cyanine Dye H-Aggregates: Both in Solution and on Au Film" *Journal of Analytical Chemistry,* **2010**, 82, 9135–9137.
47. Collie GW, Sparapani S, Parkinson GN, Neidle S. "Structural Basis of Telomeric RNA Quadruplex-Acridine Ligand Recognition" *Journal of American Chemical Society*, **2011**, 133, 2721-2728.